Journal of Environmental Chemical Engineering 13 (2025) 118686

Contents lists available at ScienceDirect

Journal of Environmental Chemical Engineering

journal homepage: www.elsevier.com/locate/jece

Insight into the adsorption of Pb^{2+} ions onto *Opuntia ficus indica* cladodes

Davide Lascari [a], Paolo Lo Meo [b], Giulio Geraci [a], Rita Lo Brutto [a], Salvatore Giovanni Michele Raccuia [c], Nicola Muratore [a], Salvatore Cataldo [a,e], Gabriele Lando [c], Ettore Madonia [d], Marilena Tolazzi [f], Andrea Melchior [f], Alberto Pettignano [a,e,*]

[a] Dipartimento di Fisica e Chimica – Emilio Segrè, Università di Palermo, Viale delle Scienze, Palermo 90128, Italy
[b] Dipartimento di Scienze e Tecnologie Biologiche, Chimiche e Farmaceutiche, Università di Palermo, Viale delle Scienze, ed. 17, Palermo 90128, Italy
[c] Dipartimento di Scienze Chimiche, Biologiche, Farmaceutiche ed Ambientali, Università degli Studi di Messina, Viale F. Stagno d'Alcontres 31, Messina 98166, Italy
[d] Dipartimento di Scienze Agrarie, Alimentari e Forestali, Università di Palermo, Viale delle Scienze, Palermo 90128, Italy
[e] NBFC, National Biodiversity Future Center, Piazza Marina 61, Palermo 90133,Italy
[f] Dipartimento Politecnico di Ingegneria e Architettura, Laboratorio di Tecnologie Chimiche, Università di Udine, Udine 33100, Italy

ARTICLE INFO

Keywords:
Lead
Opuntia ficus indica
Adsorption
Remediation
Toxic metal ions

ABSTRACT

Opuntia ficus indica cladodes (OFIC) particles were prepared from the raw material through a cost-effective treatment and used as an adsorbent for the removal of Pb^{2+} ions from aqueous solutions under different experimental conditions. The adsorbent was characterised by means of ATR-FT-IR spectroscopy, potentiometric titration, pH_{pzc}, and SEM-EDX techniques. Based on preliminary single batch adsorption experiments at different pH values, kinetics and isotherm adsorption studies were carried out fixing the pH at 5.0. Both the adsorption kinetics and thermodynamics were studied in batch without ionic medium, and in the presence of $NaNO_3$ and NaCl background salts at different ionic strengths, in the 278.15–318.15 K temperature range. The experimental conditions of the Pb^{2+} ions solution played an important role in both the affinity and the adsorption capacity of OFIC. Kinetic and isotherm adsorption data were tentatively subjected to regression analysis using diverse mathematical approaches. The pseudo second order and the Langmuir models provided satisfactory description of the kinetics and the isotherms adsorption data, respectively. Adsorption equilibrium was achieved within 150–200 min. The highest q_m value (121 mg g^{-1}) was reached at pH = 5.0, at T = 284.15 K. The adsorption process showed an activation energy of 24 kJ mol^{-1}, being endothermic and with a positive entropy change. The adsorption process was found to be reversible, and the adsorbent could be reused for at least 4 cycles, with a regeneration efficiency of 82.6 % at the fourth adsorption/desorption cycle. Breakthrough curves showed comparable adsorption behaviour under both equilibrium and non-equilibrium conditions.

1. Introduction

Pollution from toxic metal species represents a significant environmental threat due to their persistence in ecosystems and their tendency to bioaccumulate throughout the food chain [1,2]. Within this class of pollutants, lead (Pb) is particularly hazardous, as it exerts harmful effects even at low concentrations. Lead exposure is linked to a variety of adverse health effects, including neurological damage, cardiovascular diseases, kidney failure, and developmental problems in children [3,4]. In addition, lead negatively affects plant growth by inhibiting seed germination and by activating stress responses in root meristematic cells [5].

Human activities are the primary source of lead pollution, with significant contributions from industrial processes such as smelting, mining, pesticide manufacturing, and battery manufacturing. Historical practices, including the use of lead-based paints and car fuel additives, have further worsened environmental contamination [4–6]. Furthermore, untreated industrial effluents containing lead represent a major source of water pollution [7]. Wastewater streams, in which lead is usually present in its 2 + oxidation state, contain Pb^{2+} concentrations in the order of tens of mg L^{-1} [5], depending on their origin. The Pb^{2+} concentration limits recommended in drinking and wastewater by the World Health Organization (WHO), the United States Environmental Protection Agency (US-EPA), and other national agencies and

* Corresponding author at: Dipartimento di Fisica e Chimica – Emilio Segrè, Università di Palermo, Viale delle Scienze, Palermo 90128, Italy.
E-mail address: alberto.pettignano@unipa.it (A. Pettignano).

https://doi.org/10.1016/j.jece.2025.118686

Available online 13 August 2025
2213-3437/© 2025 The Authors. Published by Elsevier Ltd. This is an open access article under the CC BY license (http://creativecommons.org/licenses/by/4.0/).

organizations, range from tens of μg L^{-1} to a few mg L^{-1} [8].

To address the widespread and serious problems of toxic metal pollution, suitable wastewater management is needed. The purification process, in terms of toxicant removal, must be efficient enough to allow the release of the purified water directly into lakes, rivers and seas [9].

Currently, several conventional and advanced wastewater treatments such as chemical precipitation, coagulation, ion exchange, forwards and reverse osmosis, and membrane filtration, electrodialysis, electrodeposition, and combined decontamination techniques have been developed [5,10]. Although these decontamination approaches are widely used, they often suffer from a series of critical side effects, such as high operating costs, toxic sludge generation, use of huge amounts of chemicals, requirement of skilled labor, and low efficiency at low metal concentrations [11,12]. Hence, research has been increasingly focusing on the development of more sustainable and environment-friendly alternatives. Among the most promising decontamination strategies, adsorption processes, and particularly those based on the use of waste biomasses from the agri-food industry, have gained considerable attention due to their high efficiency, cost-effectiveness, wide availability of the natural adsorbent, and the possibility of recycling it [13–19].

Biomasses are usually used after simple, rapid and cheap chemical and physical processing, such as washing, grinding, sieving, or treatments with acids or bases. In other cases, the biomass is the precursor for the production of activated carbons or biochar. Massive literature on the topic demonstrates the versatility and effectiveness of these sorbent materials in mitigating the pollution of water contaminated by toxic metal ions [13,17,20–32]. It has been pointed out in several studies [25,26] that the adsorption capacity of biomasses for toxic metal ions is affected by various factors, including pH, ionic medium, and ionic strength of the pollutant solution, as well as the morphology and surface charge of the biomasses. Toxic metal ions can be adsorbed through two main processes: physisorption and chemisorption. Physisorption is driven by weak forces, such as Van der Waals interactions, whereas chemisorption involves the formation of stronger chemical bonds between the metal ion and the binding groups of the adsorbent [33].

This study investigates the use of *Opuntia ficus indica* cladodes (OFIC) as adsorbent material for the removal of Pb^{2+} ions from aqueous solutions. Traditionally considered agricultural waste due to their invasive nature, *Opuntia* species are increasingly recognized as a versatile and valuable resource. The several properties of their components (cladodes, fruit peels, seeds, pulp and mucilage) offer innovative solutions in different fields [34]. Different parts of *Opuntia ficus indica* (OFI) plant have been successfully employed in decontamination processes of water polluted by organic and inorganic pollutants [6,20,35,36], in the extraction of bioactive compounds in the pharmaceutical industry [37], as a nutritional resource in the food sector [38], or as source of dye and fiber in the textile industry [39].

The chemical composition of OFIC has been the object of several studies [40–42]. The main constituents are mucilage, cellulose and hemicellulose, together with lignin and a significant presence of low-molecular-weight alkali-soluble polyphenol compounds [43]. Moreover, *Opuntia* mucilage is reported to be rich in galactose, galacturonic acid, xylose, rhamnose, and arabinose residues [42,44].

Despite the growing body of research on OFI, particularly in the context of wastewater treatment,

the study of the adsorption capacity and affinity of its cladodes towards lead ions is reported only in a few articles, in which maximum adsorption capacity values ranging from 62.89 to 116.8 mg g^{-1} were reported [6,20,45]. In these works, the effects from interacting and non-interacting ionic media, the effect of ionic strength and other important aspects strictly related to the adsorption process like the Ca^{2+} ions release and the acid-base properties of the adsorbent materials remain unexplored. Moreover, the evaluation of the adsorption performance in continuous-flow fixed-bed columns has never been performed, despite this setup represents an important step towards the application of OFIC in large-scale water purification plants [46].

This work aims at filling these gaps through an in-depth adsorption study of Pb^{2+} - OFIC system. At first, the OFIC particles were extensively characterised (SEM-EDX and ATR-FTIR spectroscopy, ISE-H^+ potentiometry) to assess their surface morphology and identify their functional groups, in terms of type, concentration, acid-base properties, and their involvement in the Pb^{2+} adsorption process. Then, batch kinetic and isotherm experiments were performed, under different experimental conditions, including the initial pH (2–6), the presence of ionic medium ($NaNO_3$ and NaCl), and its ionic strength (0.1 – 0.5 mol L^{-1}), and the temperature (278.15 – 318.15 K) of Pb^{2+} ions solution. Three replicates of an isotherm experiment with different lots of OFIC particles and reagents were carried out in different labs to verify the reproducibility of the adsorption data. Gibbs and van't Hoff equations were used to calculate the ΔG^0, ΔH^0 and ΔS^0 of Pb^{2+} ions adsorption. Furthermore, column experiments including breakthrough curves with different media and ionic strengths and adsorption-desorption cycles were performed to study the adsorption efficiency in continuous flow fixed bed columns and to assess the reusability of the adsorbent material. Several models were used to analyse data obtained by kinetic, isotherm and breakthrough curve experiments. The study was complemented by OFIC's environmental impact and cost-effectiveness assessment.

2. Materials and Methods

2.1. Reagents

Pb^{2+} ion solutions were prepared by weighing the $Pb(NO_3)_2$ (Sigma Aldrich, analytical grade) salt. $NaNO_3$ (Sigma Aldrich, 99.0 %) and NaCl (Riedel-de Haën, 99.8 %) salts were dried in an oven at $T = 383.15$ K for 2 h before use. HCl, HNO_3 and NaOH used to adjust the pH of Pb^{2+} ion solutions, in potentiometric titrations, and in column adsorption/desorption experiments were prepared by diluting the following stock solutions: HCl 0.975 N (Sigma Aldrich), HNO_3 1 M (Fluka Analytical) and NaOH 1 M (Fluka Analytical) and standardised against Na_2CO_3 (Merck, 99.9 %) and $C_8H_5KO_4$ (Merck, 99.5 %), respectively, previously dried in an oven at $T = 383.15$ K for 2 h. The HCl solution used to desorb the Pb^{2+} ions from OFIC in recycle experiments, was prepared by diluting concentrated Sigma Aldrich solution.

Standard solutions of Pb^{2+} (CertiPUR, Merck) and Ca^{2+} (Titrisol, Sigma Aldrich) 1000 mg L^{-1} in 2 % HNO_3 were properly diluted and used for the construction of calibration curves. All the solutions were prepared using freshly CO_2 free ultrapure water ($\rho \geq 18$ MΩ cm) and grade A glassware.

2.2. Adsorbent preparation and characterisation

The OFI cladodes were collected in November 2023 in the countryside on the northern coast of Sicily near Palermo (Italy; 38° 6' 32.7'' N, 13° 31' 49.7'' E), roughly cut into small pieces, sun-dried for two weeks, washed thoroughly with tap water and then with ultrapure water until TOC measurements confirmed the absence of organic matter in the supernatant. The pieces of OFI cladodes were then dried in an oven at 333.15 K for two days, ground using a domestic mill, and sieved with an Octagon Digital (Endecotts) sieve shaker. OFIC particles with size in the range $0.1 < x/\text{mm} < 0.2$ were collected for the subsequent characterisation and adsorption experiments.

ATR-FT-IR spectra of OFIC particles, before and after the Pb^{2+} ions adsorption, were acquired on a PerkinElmer Spectrum Two instrument (Waltham, Massachusetts, USA) in the wavenumber range 4000–450 cm^{-1}, with a spectral resolution of 16 cm^{-1}, and accumulating 100 scans; samples were previously grinded and dried at 383.15 K for 24 h.

The microstructure of the biomass before and after the Pb^{2+} ions adsorption was assessed by field-emission scanning electron microscopy (FESEM), JEOL model JSM-7610F Plus (JEOL Ltd. Tokyo, Japan) using a

15 kV voltage and a working distance of 15 mm. Samples were previously coated with 5 nm layer of gold to increase conductivity. The microscope was equipped with energy dispersive x-ray spectroscopy probe (EDXS, Oxford Instruments) for elemental analysis.

The acid-base properties of the active sites present on OFIC samples were investigated through automatic potentiometric titrations using a Metrohm 809 Titrando plugged to a computer and a combined "sure-flow" glass electrode purchased from Orion (8172BNWP model). The sure-flow electrode was chosen to avoid clogging of the junction. The Metrohm TiAMO 2.5 software was employed to control titrant delivery, data acquisition and *e.m.f.* stability. The estimated accuracies for *e.m.f.* and titrant volume readings were ±0.15 mV and ±0.003 mL, respectively.

Suspensions of 25 cm^3 containing 0.12–1 g of material, strong inorganic acid (nitric or hydrochloric acid, $c_H = 0.01$ mol L^{-1}) to fix the pH at ~ 2.0, and background electrolyte ($NaNO_3$ or NaCl at I = 0.10 mol L^{-1}), were titrated with standard CO_2-free sodium hydroxide solutions (c_{NaOH} = 0.0997, 0.0965 mol L^{-1}) up to pH ~ 11.5 in thermostatted cells at $T = 298.15 \pm 0.1$ K.

The pH of point zero charge (pH_{pzc}) of OFIC was calculated in $NaNO_3$ 0.1 mol L^{-1}. In details, 25 mg of adsorbent particles were placed in different 50 mL Erlenmeyer flasks containing 35 mL of aqueous solution in the pH range 2 – 10. Purified N_2 gas was bubbled into each solution for 10 min. After sealing with parafilm, the suspensions were magnetically stirred for 24 h. The final pH of suspensions (pH_f) was measured and plotted against the initial pH (pH_i) calculating the pH_{pzc} as the intersection with the blank curve. All the pH measurements were done with the same potentiometric apparatus previously described.

2.3. Procedures for batch and column adsorption experiments

Initially, a series of double batch adsorption tests of OFIC particles towards Pb^{2+} ions at pH = 2, 3, 5, and 6 were performed by placing ~ 18 mg of the adsorbent in two Erlenmeyer flasks containing 20 mL of Pb^{2+} ions solution (c_{Pb2+} = 160 and 135 mg L^{-1}), at $T = 298.15$ K. The suspensions were stirred at 180 rpm for 24 h using an orbital shaker (model M201-OR, MPM Instruments) and filtered through nylon syringe filters (SPHEROS, pore size = 0.45 μm) before measuring the Pb^{2+} ions concentrations in the supernatant.

Given the similar adsorption behaviour of OFIC particles in the pH range 3–6, the initial pH was fixed at 5.0 in all subsequent batch and column experiments.

The kinetics of Pb^{2+} ions adsorption onto OFIC particles was studied in $NaNO_3$ aqueous solution, at $I = 0.1$ mol L^{-1}, in the temperature range 288.15 – 308.15 K. The OFIC particles (ca. 20 mg) were suspended in 40–75 mL of Pb^{2+} solution (c_{Pb2+} = 18 – 25 mg L^{-1}) at pH = 5.0 in a thermostatted voltammetric cell under constant and regular stirring. The metal ion concentration in the suspension was measured by Differential Pulse Anodic Stripping Voltammetry (DP-ASV) at different contact times in the time interval 0 – 9 h. The voltammetric apparatus consisted of a Metrohm 663 VA stand combined with the Autolab potentiostat, coupled with an IME663 interface, and controlled by the NOVA v. 1.10 software. The VA stand was equipped with a three-electrode system, namely i) a Multi-Mode Electrode Pro (Metrohm, code 6.1246.120) working in the Static Mercury Drop Electrode (SMDE) mode, ii) a glassy carbon auxiliary electrode (code 6.1247.000), and iii) a double junction Ag/AgCl/KCl (3 mol L^{-1}) reference electrode (code 6.0728.030). The DP-ASV measurements were performed after bubbling purified N_2 gas into the solutions for 150 s.

The isotherm experiments were carried out with Pb^{2+} aqueous solutions at $T = 298.15$ K, both without an ionic medium and in two ionic media, namely $NaNO_3$ and NaCl 0.1 mol L^{-1}. Additional isotherm experiments were carried out in NaCl 0.3 and 0.5 mol L^{-1} to evaluate the effect of chloride concentration on the adsorption performance of OFIC particles. All isotherm experiments were performed in batch mode by placing different amounts of OFIC particles (18 – 25 mg) in different Erlenmeyer flasks containing 20 mL of Pb^{2+} solution (c_{Pb2+} = 10 – 150 mg L^{-1}). The suspensions were shaken for 24 h, filtered, and the supernatants were collected for the pH (pH_f) and the equilibrium Pb^{2+} concentration (c_e) measurements. In order to confirm that adsorption equilibrium had actually been reached, additional batch control experiments were performed, in which the suspensions were filtered after 48 h. Since the adsorbent material tested in this work is a biomass, its inhomogeneity might possibly affect the replicability of the adsorption data. For this reason, three replicates of the isotherm with Pb^{2+} solution without ionic medium were carried out in different labs. In each replicate, the same OFIC mass/c_{Pb2+} ratios were used, but different lots of OFIC particles and reagents were used. Moreover, in two of the three replicates, the Ca^{2+} concentrations in the supernatants were also measured to evaluate the possible ion exchange between Pb^{2+} and Ca^{2+} ions during the adsorption process.

The reuse and recycling of the adsorbent material was investigated by packing 20 mg of OFIC particles into a glass column (2 cm diameter, 5 cm length). Glass beads were placed on top to prevent the adsorbent from moving during the experiment. Four adsorption – desorption cycles were performed. During each adsorption step, 15 mL of Pb^{2+} ions solution (c_{Pb2+} = 65 mg L^{-1} at pH = 5.0) was flowed through the column at reflux for 16 h at a flow rate of 6 mL min^{-1} (the reaching of adsorption equilibrium was verified) using a peristaltic pump (Gilson, Minipuls 3). In each subsequent desorption step, 15 mL of HCl 0.1 mol L^{-1} flowed through the column at reflux for 7 h at 6 mL min^{-1}. After each adsorption and desorption step, the adsorbent was rinsed with 100 mL of ultrapure water.

The fixed bed column experiments were carried out in a down flow system which mainly consists of a glass column (1.5 cm diameter. 18 cm length) filled with 90 mg of OFIC particles. The adsorbent bed was packed between the glass membrane at the bottom of the column and glass beads, which were used to prevent the adsorbent from rising into the solution. Air trapped between the absorbent particles was removed by passing ultra-pure water through the adsorbent bed before each experiment. A peristaltic pump (Dulabo Laborgerate, mod. PLP 380) was used to flow the Pb^{2+} ion solution (c_0 = 5 mg L^{-1}) from the top of the column, while another peristaltic pump (Gilson, mod. Minipuls 3) was placed at the exit of the column to ensure a constant flow rate. A 120-position fraction collector (BÜCHI, mod. C-660) was used to collect a volume of ~ 1.7 L of the output solution in equal fractions of 16.25 mL. The breakthrough curves experiments were carried out with Pb^{2+} solution at pH = 5.0, at $T = 298.15$ K, both without ionic medium and in the presence of$NaNO_3$ (0.1 mol L^{-1}) and NaCl (0.1 and 0.5 mol L^{-1}).

The concentrations of Pb^{2+} ions in the solutions collected during batch (isotherm) and column (reuse and recycling and breakthrough) experiments were measured by Inductively Coupled Plasma Optical Emission Spectroscopy (ICP-OES) technique using a PerkinElmer Model Optima 2100 equipped with an auto sampler model AS-90. The Pb^{2+} emission intensities were measured at the wavelength 217.00 nm and each measurement was repeated three times.

The Ca^{2+} concentration was measured by flame atomic absorption spectroscopy (FAAS) using a PerkinElmer AAnalyst 200 spectrophotometer. The Ca^{2+} absorption was measured at the wavelength 422.67 nm and each measurement was repeated three times.

Calibration curves were built in the same experimental conditions and covering the metal ion concentration range of adsorption experiments.

The pH of the Pb^{2+} solutions, before and after contact with the OFIC particles, in the kinetic and isotherm experiments was measured with the previously described potentiometric apparatus.

2.4. Kinetic, isotherm, and column models for Pb^{2+} adsorption onto OFIC particles

The kinetic data of Pb^{2+} ions adsorption onto OFIC particles were tentatively fitted with several kinetic models. At first, the widely used

pseudo-first order (PFO) equation of Lagergren [47] (Eq. (1)) and the pseudo-second order (PSO) equation [48] Eq. (2) were tested:

$$\frac{dq_t}{dt} = k_1(q_e - q_t) \quad (1)$$

$$\frac{dq_t}{dt} = k_2(q_e - q_t)^2 \quad (2)$$

where q_t and q_e represent the adsorption capacity of OFIC particles (mg g^{-1}) at time t and at the equilibrium, respectively; k_1 (min^{-1}) and k_2 (g mg^{-1} min^{-1}) are the rate constants of adsorption in the PFO and PSO equations. The corresponding integrating non-linear equations under boundary conditions $t = 0$ to $t = t$ and $q_t = 0$ and $q_t = q_t$ used in data processing are listed below:

$$q_t = q_e \quad (1 - \quad e^{-k_1 t}) \quad (3)$$

$$q_t = \quad \frac{q_e^2 \quad k_2 \quad t}{1 + q_e \quad k_2 t} \quad (4)$$

Moreover, considering the great number of different binding sites present in the OFIC particles and their possible involvement in Pb^{2+} adsorption, the general pseudo n order (PGO) model [49] was also tested. Its integrated form for the same boundary conditions is reported in the Eq. (5):

$$q_t = q_e - \frac{q_e}{(k_n q_e^{(n-1)} t(n-1) + 1)^{\frac{1}{(n-1)}}} with \quad n \quad \neq 1 \quad (5)$$

where k_n (min^{-1} (g mg^{-1})$^{n-1}$) and n are the rate constant and the general order of adsorption, respectively.

The equilibrium data of Pb^{2+} adsorption on OFIC collected through batch experiments were processed with Freundlich [50] (Eq. (6)) and Langmuir [51] (Eq. (7)) isotherm models:

$$q_e = \quad K_F \quad c_e^{1/n} \quad (6)$$

$$q_e = \quad \frac{q_m \quad K_L \quad c_e}{1 + K_L \quad c_e} \quad (7)$$

where q_m (mg g^{-1}) is the maximum adsorption capacity of the OFIC particles, c_e (mg L^{-1}) is the equilibrium concentration of Pb^{2+} in each solution; K_F ($L^{1/n}$ g^{-1} $mg^{1-1/n}$) and K_L (L·mg^{-1}) are the constants of Freundlich and Langmuir models, respectively.

The Pb^{2+} ions adsorption capacity at different contact times t (q_t) and at equilibrium (q_e) were calculated by the Eq. (8):

$$q_t or q_e = \quad \frac{V \quad (c_0 - c_t)}{m} \quad (8)$$

where V (L) is the volume of the Pb^{2+} ion solution and m is the mass of OFIC particles (g); c_0 and c_t are the Pb^{2+} ion concentrations in the solutions (mg L^{-1}) at $t = 0$ and $t = t$, respectively. To calculate q_e, in Eq. (8) c_t was replaced with the equilibrium concentration (c_e).

The kinetic constant values (in $NaNO_3$ 0.1 mol L^{-1}, pH = 5.0) in the temperature range 278.15–308.15 were used to calculate the activation energy of adsorption (E_a) (kJ mol^{-1}) by using Arrhenius equation (Eq. (9)):

$$\ln k_2 = \quad -\frac{E_a}{RT} + \ln A \quad (9)$$

where R is the universal gas constant 8.314 J mol^{-1} K^{-1}, A is the Arrhenius coefficient or pre-exponential factor (g mg^{-1} min^{-1})

The Langmuir constant values (c_{Pb}^{2+} in mol L^{-1}) [52] at different temperatures were used to calculate the thermodynamic parameters ΔG^0 (kJ mol^{-1}), ΔH^0 (kJ mol^{-1}) and ΔS^0 (kJ mol^{-1} K^{-1}) by using Gibbs (Eq. (10)) and van't Hoff (Eq. (11)) equations. The following assumptions were done: i) the adsorption is reversible, ii) the stoichiometry of adsorption does not change; iii) equilibrium condition is established during adsorption experiments [53,54].

$$\Delta G^0 = \quad -RT\ln K_L \quad (10)$$

$$\ln K_L = \quad -\frac{\Delta H^0}{RT} + \frac{\Delta S^0}{R} \quad (11)$$

where T is the temperature in K.

The Logistic (Eq. (12)), Gompertz (Eq. (13)) and Log-Gompertz (Eq. (14)) models in their nonlinear form[55] were used to fit the breakthrough curves of Pb^{2+} ions adsorption of OFIC particles:

$$\frac{c_t}{c0} = \frac{1}{1 + \exp(a - bt)} \quad (12)$$

$$\frac{c_t}{c0} = \exp\left[-\exp(\alpha_G - \beta_G t)\right] \quad (13)$$

$$\frac{c_t}{c0} = \exp\left[-\exp(\alpha_{LG} - \beta_{LG}\ln t)\right] \quad (14)$$

where a, b (min^{-1}) are the parameters of the logistic model while α_G, β_G (min^{-1}) and α_{LG}, β_{LG} ($(\ln min)^{-1}$) are the Gompertz and Log-Gompertz model parameters, respectively. The Eq. (12) corresponds to the simplified Bohart-Adams model [56] which is mathematically equivalent to both the Thomas and Yoon-Nelson models [55]. Therefore, a and b can be related to the parameters of those models as reported elsewhere [55]. While the simplified Bohart-Adams model and the Thomas and Yoon-Nelson models reduce to the same logistic function being derived from similar starting assumptions, the Gompertz and Log-Gompertz models have been proposed on largely empirical bases [57].

OriginLab suite software (OriginLab Corporation, Northampton, Massachusetts, USA) was used to fit kinetic, isotherm and breakthrough models to experimental data.

3. Results and discussion

3.1. Opuntia Ficus Indica Cladodes: chemical and morphological characterisation

The OFIC particles showed a pH_{pzc} of 5.49 in $NaNO_3$ 0.1 mol L^{-1} (see Fig. 1). This indicates that, under these conditions, the surface of the OFIC particles has a net positive or negative charge at pH values below or above 5.49, respectively. It can be reasonably assumed that nearly the same occurs also in other ionic media, even under different ionic strength conditions. The surface charge is the consequence of

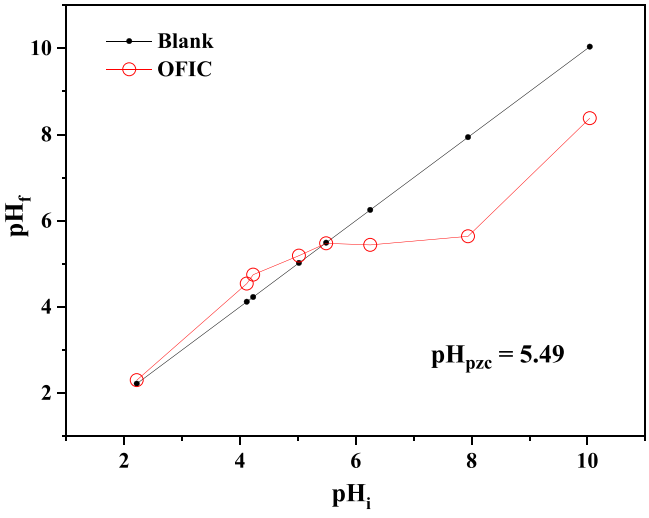

Fig. 1. pH_{pzc} of OFIC in $NaNO_3$ 0.1 mol L^{-1}.

protonation/deprotonation equilibria involving the functional groups of the adsorbent material that, as known, is a natural biomass containing a variety of macromolecules. Hence, the definition of its acid-base properties is indeed a challenging task.

For example, it has been demonstrated that, in the case of a synthetic polyelectrolyte such as polyacrylic acid [58], the acid-base properties can be interpreted in terms of dissociation degree, under the assumption that the deprotonation of a carboxylic group may influence the deprotonation of a vicinal carboxylic group and so on, or, alternatively, that the polyelectrolyte can be considered as a discrete bicarboxylic acid units.

Here, acid-base properties of OFIC particles were studied by potentiometry in a wide pH range (2.0–11.5) both in NaCl and $NaNO_3$ ionic media. The analysis of the potentiometric titrations was performed by means of the BSTAC software (version 4.0) [59], varying the pH range, but also considering monoprotic and diprotic functional groups. Together with the acidic constants, the site density ($OFIC_i$, mmol g^{-1}) was estimated by multiplying the refined site concentration (c_{OFICi}, mmol L^{-1}) during the titration analysis by the volume of the titrand solution (L) and dividing the resulting mole amount by the mass of OFIC used in the titration (g) as in Eq. 15. The site density (not the site concentration) should, in principle, be independent of the amount of OFIC used in each titration, so that this calculation was used as a measure of the reliability of the data analysis.

$$\text{Site density } (OFIC_i, \text{ mmol } g^{-1}) = c_{OFICi}, (\text{mmol } L^{-1})\ \text{Volume (L)} / \text{OFIC mass (g)} \quad (15)$$

A detailed description of the results obtained, in terms of protonation constant models, by processing the potentiometric data of the entire pH range investigated is reported in Tables S1 – S4 and Figures S1 and S2 of Supplementary Materials.

Due to dissolution phenomena that involve the adsorbent particles at alkaline pH, the most reliable results were obtained for the adsorbent sites titrated in the pH range $2 \leq pH \leq 6$ [60]. Under these pH conditions, biomasses like the one used in this work are generally used for the recovery of metal cations. Most likely, the proton donor sites in this pH range, indicated hereinafter by the acronym $OFIC_1$, are carboxylic groups. The dissociation constants and the concentrations of $OFIC_1$ sites refined in both ionic media are summarized in Table 1. The dissociation constant obtained in $NaCl_{(aq)}$ is apparently lower than that in $NaNO_{3(aq)}$. The site density obtained considering all titrations is $OFIC_1 = 0.39 \pm 0.06$ mmol g^{-1} (95 % C.I.).

Morphological characterisation of the OFIC biomass was achieved by SEM Techniques. The micrographs of OFIC particles at 1000x magnification, before and after adsorption of Pb^{2+} ions, are shown in Fig. 2, together with the relevant EDX spectra. The biomass consisted of particles with irregular shapes, a corrugated and wrinkled surface and a variable size in the range of 0.1–0.2 mm. The adsorption of lead ions does not cause significant changes on the material surface.

Table 1
Summary of the results of the data analysis of the potentiometric titrations of OFIC in $NaCl_{(aq)}$ and $NaNO_{3(aq)}$ ionic media at $T = 298.15$ K, pH range: 2 – 6, assuming only one acid-base functional group ($OFIC_1$).

Medium	Mass(g)	$\log K^H$	c_{OFIC1} [a]	$[H]_T$ [b]	MD_{fit} [c]
	0.1518		2.54	8.0	
NaCl	0.2025	3.49 ± 0.01	3.76	8.4	0.56
	0.2996		4.91	8.7	
	0.1293		3.03	9.4	
$NaNO_3$	0.4998	3.67 ± 0.01	7.83	8.6	1.04
	0.7009		9.13	8.3	
	1.0010		12.31	9.1	

[a] in mmol L^{-1}
[b] analytical concentration (mmol L^{-1}) of proton obtained by the acid-base titration
[c] mean deviation of the fit (in mV).

The elemental composition of OFIC calculated in % (w/w) by the EDX spectra registered before and after the toxic metal ion adsorption is reported in Table 2. Although these results are only semi-quantitative, it can be noticed that the adsorption of lead ions is accompanied by a release of calcium, suggesting an adsorption mechanism based at least in part on ion exchange.

Interesting and useful information regarding the interaction between the biomass and the Pb^{2+} ion can be suitably achieved by ATR-FTIR spectroscopy. The spectrum of OFIC (Fig. 3) features various signals, accounting for the different components present in the plain biomass. Detailed signal attributions can be confidently done based on literature reports [43,44,61], and are summarized in Table 3 for reader's convenience. Along with the wavenumber regions 3700–2700 cm^{-1}, (featuring the O-H, N-H and C-H stretching vibrations) and 1200–900 cm^{-1} (polysaccharide fingerprints), the most interesting signals are those around 1612 (carboxylate stretching), 1315 (-OH in-plane bending) and 780 (galactose ring vibration) cm^{-1}.

The adsorption of the metal ion causes some significant spectral changes in the fingerprint region, which can be clearly evidenced by calculating the difference spectrum before and after the adsorption experiment (green line in Fig. 4). In particular, it is easy to notice a significant shape modification of the carboxylate signal at 1612 cm^{-1}, which reveals, upon deconvolution analysis, the superimposition with a new signal centered at 1569 cm^{-1}. The latter value is reasonably close to the one found for lead acetate trihydrate (namely, 1559 cm^{-1}) [62], providing unambiguous evidence for the interaction between the Pb^{2+} ion and the carboxylate groups present in the biomass, likely those in the galacturonic acid residues of the mucilage component. Furthermore, two new signals appear at 1288 and 772 cm^{-1}, i.e. in the –OH bending and galactose ring vibration regions, which suggest the occurrence of a significant interaction between the metal ion and the hydroxyl groups of the various biomass polysaccharides.

3.2. Kinetics of Pb^{2+} ions adsorption onto OFIC

The kinetics of Pb^{2+} ions adsorption onto OFIC particles was studied at pH = 5.0, in $NaNO_3$ 0.1 mol L^{-1} in the temperature range 278.15 – 308.15 K. For each temperature, two or three kinetic experiments were carried out with small changes in the OFIC-to-c_{Pb2+} ratio (see Section 2.3 for experimental details). The acid-base properties of OFIC particles (see Section 3.1) suggested the possible involvement of different binding sites, mainly carboxylic groups, during the adsorption process and the possibility of a kinetic adsorption process of order higher than two. For this reason, the experimental data were processed with the most used PFO and PSO kinetic equations and also with the PGO model. The latter one has already been used by several authors [49,63,64] and provides a non-predetermined adsorption order (n).

At first, all datasets were individually processed with the three kinetic models. Considering the negligible differences in refined parameters values (k_1, k_2, k_n, n) from datasets at the same temperature, they have also been subjected to a simultaneous multiparameter fitting procedure, providing the refinement of a unique common kinetic constant value and, in the case of the PGO model, a single n value at each temperature. The resulting optimized parameters values and the relevant fitting statistics for the three kinetic models are reported in Table S5 of Supplementary Materials.

The goodness of fit increases moving from PFO to PSO model suggesting a reaction order higher than one. Although the adjusted R^2 values obtained with the PGO model were slightly larger, the kinetic equation chosen as the best model was the PSO (see Table 4). Indeed, the slight improvement in the goodness of fit of the PGO model was attributed to the fact that the PGO is the only three-parameter model among those considered. Furthermore, the data fit with the PGO model produced anomalous and trendless values for both the kinetic constant (k_n) and the reaction order (n), which makes the PGO model unreliable.

The kinetic data at the four temperatures investigated are depicted,

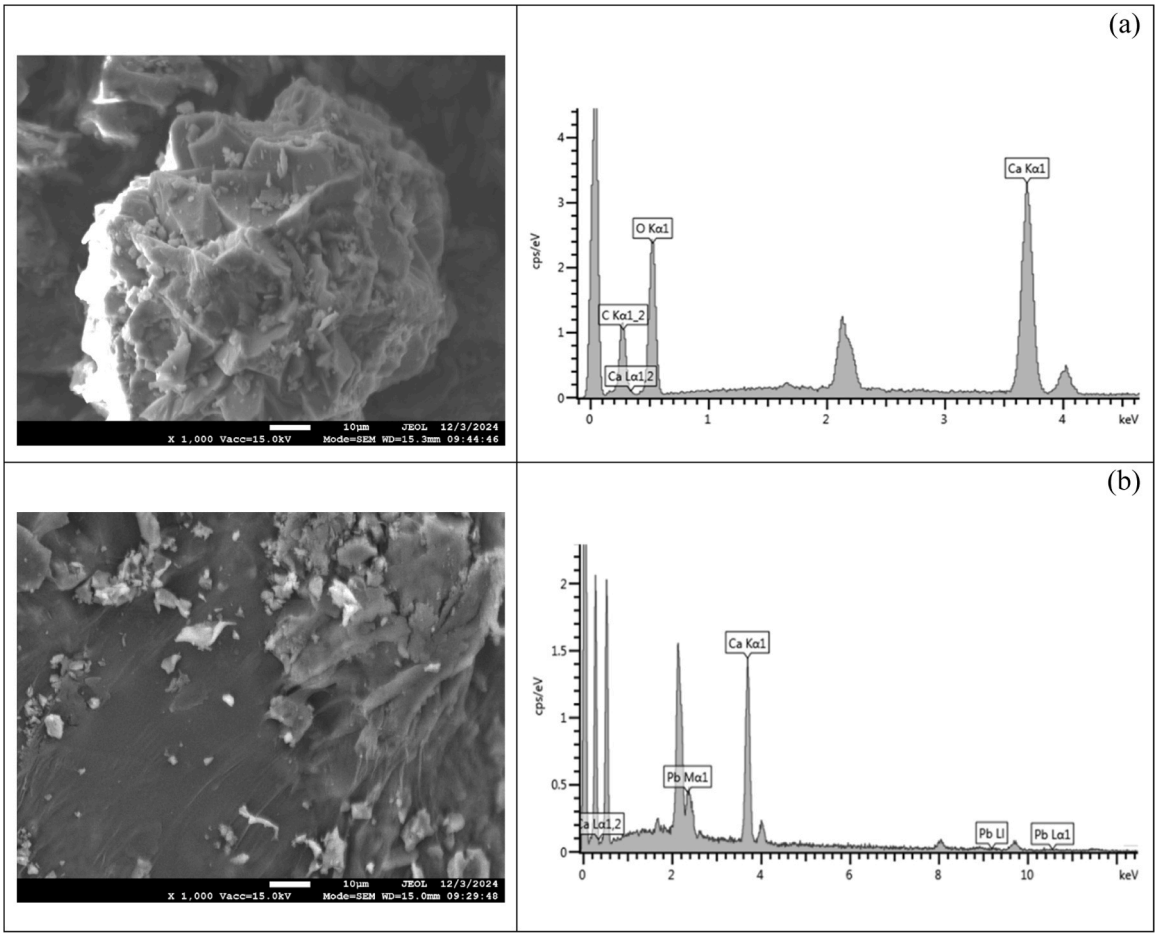

Fig. 2. SEM micrographs at 1000x magnification and EDX spectra of OFIC particles before (a) and after Pb^{2+} ions adsorption (b).

Table 2
Elemental composition of OFIC particles before and after Pb^{2+} adsorption from EDX spectra analysis[a].

Samples	Elemental composition (w/w %)			
	C	O	Ca	Pb
OFIC	15.0 ± 1.8[b]	51.9 ± 1.6[b]	33.1 ± 3.3[b]	-
OFIC-Pb^{2+}	49 ± 15	36.0 ± 6.8	9 ± 8	6.0 ± 1.9

[a] the percentages are the average of five EDX analysis
[b] ± std. dev.

together with the fit curves of the three kinetic models, in Fig. 5 ($T = 278.15$ K) and in Fig. S3 of Supplementary Materials. The adsorption equilibrium was reached within 150/200 min, with small differences at the different temperatures. The kinetic constant (k_2) values increase with increasing of temperature going from $1.026 \cdot 10^{-3}$ g mg^{-1} min^{-1} at $T = 278.15$ K to $2.711\ 10^{-3}$ g mg^{-1} min^{-1} at $T = 308.15$ K (see Table 4). From the obtained k_2 data, the activation energy (E_a) of the adsorption process was easily retrieved by applying the Arrhenius equation (Fig. 6). In adsorption studies, the activation energy represents the boundary energy that must be overcome for a specific adsorbate to be adsorbed on the surface of a specific adsorbent. Hence, its value can

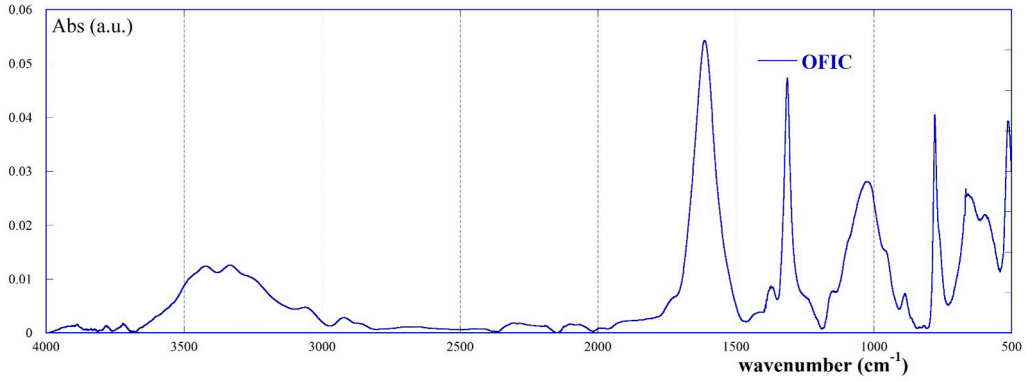

Fig. 3. Complete ATR-FTIR spectrum of plain OFIC (4000–500 cm^{-1}).

Table 3
Attribution of ATR-FTIR signals.

Signal (cm^{-1})	Attribution
3419, 3333, 3250	-OH str., -NH_2 str.
3057	Aromatic CH str.
2927, 2851	Aliphatic CH str.
1612	Asymm. –COO^- str.
1315	Cellulose/hemicellulose -OH in-plane bend.
1151	Cellulose C-O-C glycosidic bond asymm str.
Several superimposed bands around 1027	Cellulose/hemicellulose C-OH str.
780	Mucilage galactose ring vibration

help to assess the adsorption mechanism. Indeed, it is recognized that an activation energy value lower or higher than a threshold value estimated in the range of 40 [65–67] to 50 [68–71] kJ mol^{-1} indicates an adsorption process based mainly on physisorption or chemisorption, respectively. Therefore, considering the E_a value of 24 ± 2 kJ mol^{-1} obtained in this work for the Pb^{2+} ions adsorption onto OFIC particles, the adsorption process can be considered a physisorption process in which the toxic metal ions are adsorbed through ionic interactions of different strength (van der Waals, ion exchange, etc.) with the binding groups of OFIC which are more or less protonated or salified with Ca^{2+} ions depending on the solution pH (see the results of OFIC characterisation reported in Section 3.1).

3.3. Adsorption equilibria of Pb^{2+} onto OFIC

Some preliminary batch adsorption tests were carried out with Pb^{2+} aqueous solutions at pH = 2.0, 3.0, 5.0, and 6.0 and at T = 298.15 K. The experiments were performed at the same OFIC mass to $c_{Pb^{2+}}$ ratios corresponding to the adsorbent saturation conditions (right side of isotherm, $q_e \rightarrow q_m$). The results obtained in terms of q_e vs. pH are reported in the histogram of Fig. 7. Surprisingly, the adsorption capacity of OFIC at the same OFIC mass to c_{Pb2+} ratios had a high and constant value over a fairly wide pH range (3 – 6), decreasing only at pH = 2.0, i.e. under conditions providing a strong competition between H^+ ions and Pb^{2+} ions for the binding sites of the adsorbent material.

No significant pH variation was found for batch experiments at pH = 2.0 and 3.0. When the same amount of OFIC particles is put in water at pH 5 or 6, the protonation of $OFIC_1$ sites (see acid-base properties of OFIC in section 3.1 and in Supplementary Materials) of the material causes an increase in pH values up to 6.1 and 6.4, respectively. At the same initial pH, when Pb^{2+} ions are added to the solutions, the pH at adsorption equilibrium was 5.1 and 4.8, respectively. These findings indicate that the Pb^{2+} ions adsorption involves an ion exchange between the protons of $OFIC_1$ sites and the metal ion.

Then, pH 5.0 was chosen to study the thermodynamics of Pb^{2+} ions adsorption, carrying out several isotherm experiments in batch with toxic metal ion solutions without ionic medium, in $NaNO_3$ 0.1 mol L^{-1} and in NaCl at different concentrations (0.1, 0.3 and 0.5 mol L^{-1}), and in the temperature range 284.15 – 318.15 K. Relevant data were processed with the Langmuir and Freundlich isotherm models. Fitting parameter values are collected in Table 5, together with the mean pH value measured in the suspensions at the adsorption equilibrium (pH_f), the effective maximum adsorption capacity ($q_{m\ exp}$) and the statistical

Table 4
Parameters of PSO kinetic equation for Pb^{2+} adsorption onto OFIC particles in aqueous solution containing $NaNO_3$ 0.1 mol L^{-1}, at pH = 5.0, and at different temperatures in the range 278.15 ≤ T / K ≤ 308.15.

T / K	OFIC[a]	$c_{Pb^{2+}}$[b]	V[c]	q_e[d]	k_2[e]	adj. R^2
278.15	18.3	20.35	50	34.0 ± 0.1	(1.026 ± 0.014) 10^{-3}	0.9974
	18.5	17.91	40	34.6 ± 0.1		
	25.3	24.98	40	36.6 ± 0.1		
288.15	20.2	21.34	50	33.9 ± 0.2	(1.313 ± 0.032) 10^{-3}	0.9916
	18.4	21.26	50	33.3 ± 0.2		
298.15	25.2	20.44	75	35.2 ± 0.3	(2.033 ± 0.079) 10^{-3}	0.9873
	18.3	20.53	50	39.4 ± 0.3		
308.15	18.0	17.95	50	25.7 ± 0.1	(2.711 ± 0.060) 10^{-3}	0.9940
	20.9	19.11	50	26.1 ± 0.1		

[a] mg of OFIC particles
[b] in mg L^{-1}
[c] in mL
[d] mg g^{-1}, ± std. dev.
[e] (g mg^{-1} min^{-1}), ± std. dev.

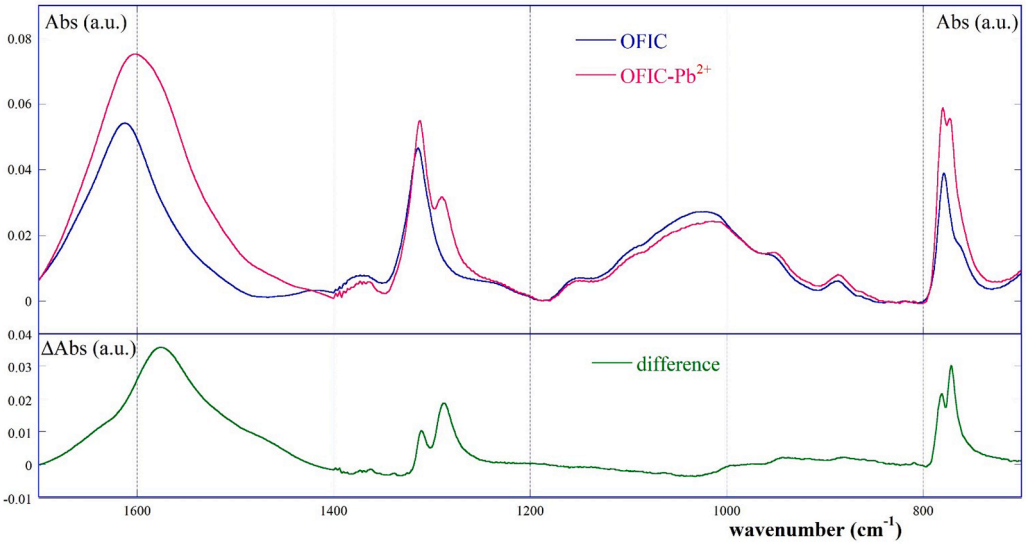

Fig. 4. Section of the ATR-FTIR spectra (1700–700 cm^{-1}) of OFIC before (blue line) and after (red line) the interaction with Pb^{2+} ions, and difference spectrum (after suitable baseline correction and normalization, green line).

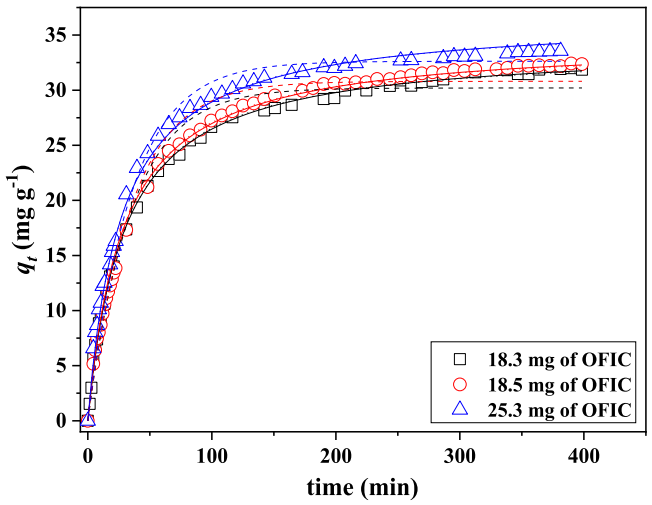

Fig. 5. Dependence of q_t (mg g^{-1}) on contact time for the Pb^{2+} ions adsorption onto OFIC particles from solution containing $NaNO_3$ 0.1 mol L^{-1}, at pH = 5.0, at 278.15 K. Data are fitted with PFO (dashed line) PSO (continuous line), and PGO (dotted line) kinetic equations.

parameter R^2. The experimental data plot (q_e vs c_e) and the fitting curves obtained with the two isotherm models are depicted in Fig. 8 and in Fig. S4 of Supplementary Materials. Better fitting quality was achieved with the Langmuir equation. The suitability of the Langmuir model was also confirmed by the agreement between the $q_{m\ exp}$ values and the theoretical q_m values calculated from the isothermal model (see Table 5) [72]. According to this isotherm model, the Pb^{2+} ions were adsorbed by OFIC through equivalent sites, presumably the carboxylic groups, which form a monolayer on the surface of the adsorbent material after saturation.

Beyond the general speculations on the adsorption mechanism, related to the empirical isotherm model that best fits the experimental data, the analysis of the fitting parameters of the Langmuir isotherm was very useful to predict and optimize the adsorption process at the experimental conditions of the pollutant solution. In particular, the highest adsorption ability of OFIC particles was found with Pb^{2+} solution at low ionic strength, and at T = 284.15 K (q_m = 121 mg g^{-1}). By increasing the temperature, the adsorption capacity decreases down to the value of 88 mg g^{-1} at 318.15 K. This trend of the q_m can be attributed to a change in the adsorbent texture, which makes some sites of the material incapable of binding the metal ion [73]. The addition of $NaNO_3$ 0.1 mol L^{-1} to the Pb^{2+} solution causes a decrease in the q_m value (to 92 mg g^{-1}) that can be ascribed to the shielding effect of the ions present in the ionic medium dissociation, and to the competition of Na^+ ions for the binding sites of the adsorbent. In the presence of NaCl, at the same ionic strength, the adsorption ability of OFIC undergoes a further decrease because the above-mentioned effects are combined with the interaction of the Pb^{2+} ions with the chloride ions from the ionic medium dissociation. This results in the formation of chlorinated species of the Pb^{2+} ion ($PbCl^+$, $PbCl_2$, $PbCl_3^-$) having different size and charge, and thus different ability to interact with OFIC particles. The latter conclusion is supported by the particularly low q_m value found in NaCl 0.3 mol L^{-1}. It is interesting to notice that, by further increasing the NaCl concentration up to 0.5 mol L^{-1}, a modest increase in the adsorption capacity of OFIC can be observed remains at low values but slightly higher than that observed in NaCl 0.3 mol L^{-1}. In order to rationalize the effect of chloride, the trends of the q_m, K_L, and of the formation percentages of the Pb^{2+} species vs. c_{Cl^-} were depicted in Fig. 9a and b. The formation percentages of the Pb^{2+} species were calculated from the distribution diagrams constructed with formation constants from the literature [74]. The highest q_m value occurs when 100 % of the lead is present as Pb^{2+} aquo ion (low ionic strength), and q_m decreases with the same trend as the sum of the formation percentages of positively charged lead species (Pb^{2+} and $PbCl^+$). The slight increase of q_m in NaCl 0.5 mol L^{-1} may be tentatively attributed to the formation of the $PbCl_3^-$ species, the only negatively charged lead species, that reaches 12.4 % and is able to electrostatically interact with the OFIC surface, which is positively charged at pH = 5 (pH_{pzc} = 5.49).

The K_L value decreases with increasing chloride concentration, showing a trend very similar to that of the aquo ion of the metal ion (see Fig. 9b). This indicates the greater affinity of OFIC particles towards the aquo ion, the lead species with the highest positive charge. The appreciable affinity of OFIC towards the toxic metal in NaCl 0.5 mol L^{-1} is attributable to the high formation percentage of the other positively charged lead species ($PbCl^+$), which, together with the negligible percentage of aquo ion reach the 46 % (see Fig. 9b).

As hypothesized on the basis of the kinetic results, the mechanism of Pb^{2+} ions adsorption onto OFIC is a physical adsorption based on ion exchange between the Pb^{2+} ions (or other positively charged lead species) and the Ca^{2+} ions of OFIC particles (see semi-quantitative elemental analysis of the material obtained from EDX spectra) and on weak electrostatic interactions between the metal ion and the carboxylic

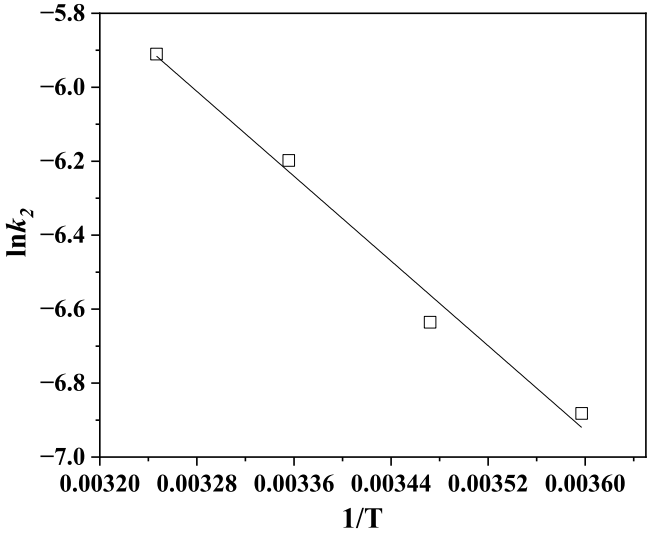

Fig. 6. Arrhenius plot for the Pb^{2+} ions adsorption onto OFIC particles from aqueous solutions containing $NaNO_3$ 0.1 mol L^{-1}, at pH = 5.0 in the temperature range 278.15 – 308.15 K.

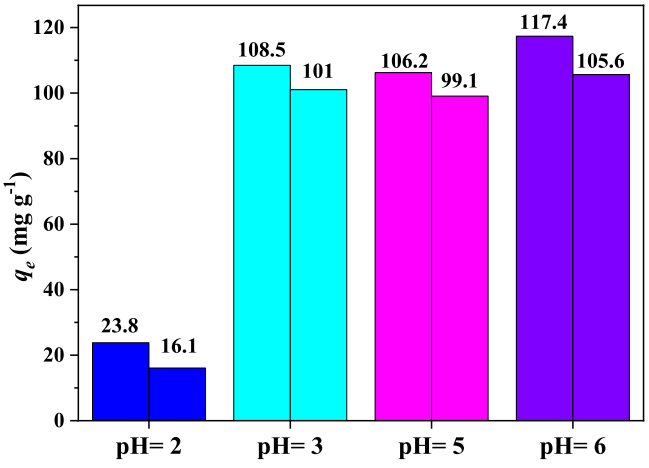

Fig. 7. q_e values of Pb^{2+} adsorption onto OFIC particles in aqueous solution at pH = 2.0, 3.0, 5.0, and 6.0. Experimental conditions: ~ 18 mg of OFIC particles in 20 mL of Pb^{2+} solution (c_{Pb2+} = 160 and 135 mg L^{-1}) at T = 298.15 K.

Table 5
Freundlich and Langmuir isotherm parameters for the Pb^{2+} ions adsorption onto OFIC particles at pH = 5.0, without ionic medium ($I \rightarrow 0$ mol L^{-1}), in $NaNO_3$ 0.1 mol L^{-1} and in NaCl 0.1 – 0.5 mol L^{-1}, and in the temperature range 284.15 – 318.15 K.

					Langmuir Model			Freundlich Model		
Ionic medium	***I* (mol L^{-1})**	**pH_f[a]**	***T* / *K***	**$q_{m\ exp}$[b]**	**q_m[c]**	**K_L[d]**	**adj. R^2**	**K_F[e]**	***n***	**adj. R^2**
none	I → 0	5.2	284.15	114 ± 3	121 ± 6	0.26 ± 0.07	0.9549	43 ± 4	4.0 ± 0.4	0.9682
		5.1	298.15	107 ± 3	113 ± 4	0.33 ± 0.04	0.9615	41 ± 3	4.0 ± 0.3	0.9552
		5.1	318.15	90 ± 3	88 ± 3	0.42 ± 0.07	0.9777	34 ± 3	3.9 ± 0.5	0.9581
$NaNO_3$	0.1	5.2	298.15	80 ± 2	92 ± 2	0.08 ± 0.01	0.9843	19 ± 2	3.0 ± 0.3	0.9172
NaCl	0.1	5.9	298.15	71 ± 2	72 ± 2	0.25 ± 0.03	0.9875	22 ± 3	3.9 ± 0.4	0.9708
NaCl	0.3	5.8	298.15	35 ± 1	35.7 ± 0.8	0.19 ± 0.02	0.9932	13.0 ± 0.9	4.2 ± 0.4	0.9872
NaCl	0.5	5.4	298.15	46 ± 1	48 ± 1	0.15 ± 0.02	0.9943	16 ± 3	4.4 ± 0.8	0.9651

[a] mean pH value at adsorption equilibrium
[b] effective maximum adsorption capacity (last experimental q_e value on the right side of the isotherm)
[c] mg g^{-1}
[d] L mg^{-1}
[e] $L^{1/n}$ g^{-1} $mg^{1-1/n}$.

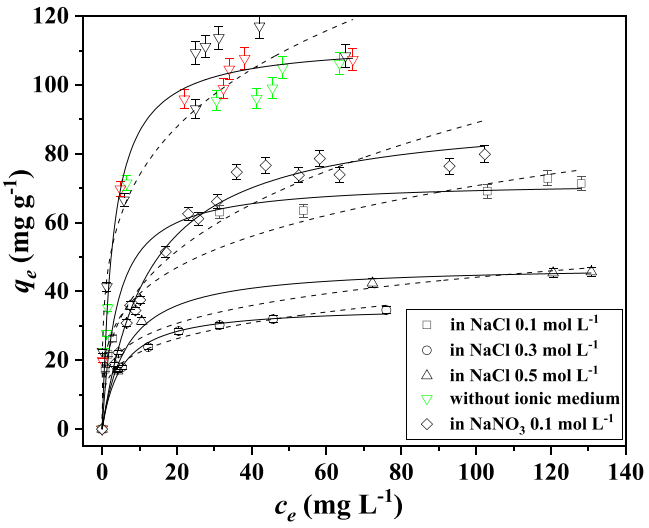

Fig. 8. Adsorption isotherms of Pb^{2+} onto OFIC particles from aqueous solution at pH = 5.0, without ionic medium (three replicates indicated with black, red and green symbols) and with the addition of $NaNO_3$ or NaCl salts at different concentrations, and $T = 298.15$ K. Experimental data were fitted with Freundlich (dashed lines) and Langmuir (continuous lines) models.

and hydroxyl groups of the adsorbent (see ATR-FTIR spectra of OFIC acquired before and after Pb^{2+} ions adsorption). To confirm the Ca^{2+} - Pb^{2+} ion exchange mechanism proposed, the Ca^{2+} ions released from OFIC particles during Pb^{2+} adsorption were monitored in two replicates of the adsorption isotherm experiments at pH = 5.0 and at $T = 298.15$ K. The q_e values of the Pb^{2+} adsorbed and Ca^{2+} released (both in mmol g^{-1}) by OFIC vs. c_e of Pb^{2+} (mmol L^{-1}) are reported in Fig. S5 of Supplementary Materials. The adsorption of Pb^{2+} ions by OFIC particles is actually accompanied by a gradual release of Ca^{2+} ions. In particular, the mole amount of Pb^{2+} ions adsorbed per gram of OFIC particles is slightly higher than the Ca^{2+} released in all the isotherm ($q_{m\ (Pb^{2+}\ adsorbed)} = 0.56 \pm 0.02$ mmol g^{-1} and $q_{m\ (Ca^{2+}\ released)} = 0.41 \pm 0.01$ mmol g^{-1}). This finding confirms that the mechanism of Pb^{2+} adsorption is physisorption, mainly based on ionic exchange. The difference between Pb^{2+} adsorbed and Ca^{2+} released correspond to the Pb^{2+} adsorbed by weak electrostatic interactions between the toxic metal ion and the adsorbent surface.

Further confirmation of the adsorption mechanism comes from the pH_f values (average pH of solutions at adsorption equilibrium) measured for each adsorption isotherm experiment and in lead-free aqueous solutions at initial pH = 5.0 after contact with the same amounts of OFIC particles of isotherm experiments. The highest pH_f was found in lead-free solutions (6.1) followed by the pH_f values of solutions coming from adsorption isotherm experiments in NaCl (5.9, 5.8 and 5.4), in $NaNO_3$ 0.1 mol L^{-1} (5.2) and without ionic medium (5.1). The lower the amount of Pb^{2+} ions adsorbed by OFIC particles the higher the pH_f is (higher H^+ - Ca^{2+} ionic exchange between solution and OFIC particles) and, consequently, the higher the amount of Pb^{2+} ions adsorbed by OFIC

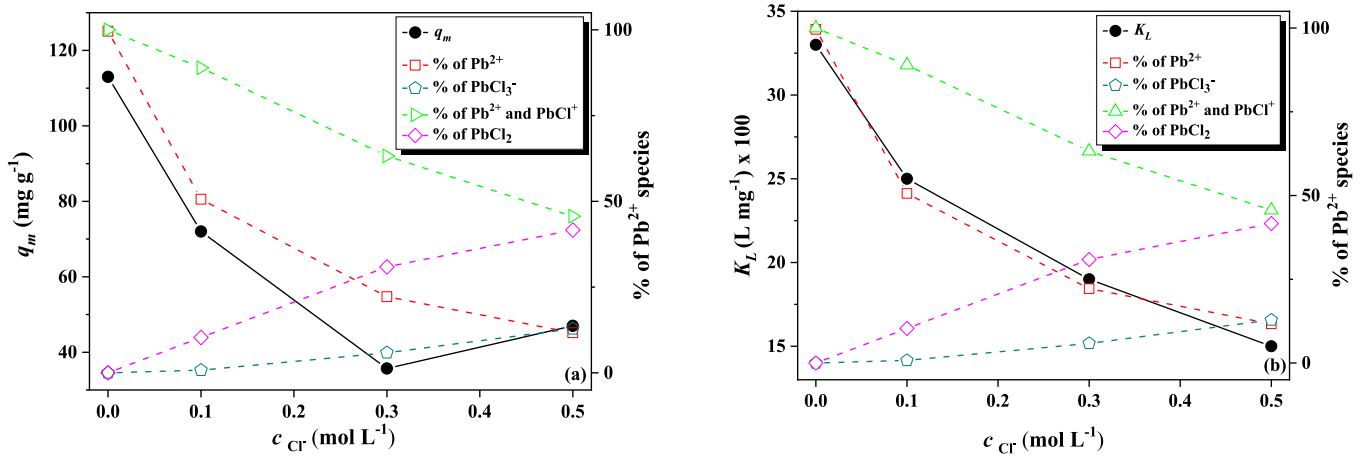

Fig. 9. Trend of q_m values and of formation percentages of Pb^{2+} species as a function of chloride concentration in solution (9a); trend of K_L values and of formation percentages of Pb^{2+} species as a function of chloride concentration in solution (9b).

the higher the Pb^{2+} - Ca^{2+} ionic exchange is (lower amount of H^+ bounded to OFIC).

3.4. Reproducibility of isotherm adsorption data

Although the material preparation and the isotherm experiment protocols were carefully followed, the intrinsic inhomogeneity of biomasses as well as random errors related to solutions preparation, dilutions, and so on may cause differences in the obtained experimental results (*i.e.*, biased c_e and q_e values). Therefore, to verify the reproducibility of the obtained results three replicates of the adsorption isotherm experiment at low ionic strength, at pH = 5.0 and T = 298.15 K, namely PA1, ME2 and ME3, were carried out. In detail, the experiments were performed in two different labs (Palermo and Messina, Italy), taking care that each experiment was totally independent of the other in terms of reagents and lot of OFIC particles used. The experimental data collected were independently and simultaneously analysed using the Langmuir model, and the corresponding parameter values are reported in Table S6 of the Supplementary Materials. Welch *t*-test was conducted to compare the q_m and K_L values across the three replicates by using the eq. S1 (see Supplementary Materials) with a null hypothesis (H_0) that there is no significant difference between the sets and an alternative hypothesis (H_1) that there is a significant difference between them (*e.g.*, H_0: q_m (PA1) = q_m (ME2); H_1: q_m (PA1) ≠ q_m (ME2)). In each comparison, both the experimental *t*-value (t_{exp}) for q_m and K_L were lower than the critical *t*-value (t_{crit}) at a 95 % confidence level, indicating that there were no statistically significant differences among the independent replicates.

Furthermore, when the results from the individual replicates were compared with those obtained through a global fitting approach, using a simultaneous multi-parameter fitting procedure that refined a single common q_m and K_L value for all three replicates, the statistical analysis confirmed that the parameters calculated from the individual replicates did not significantly deviate from those obtained from the global fit. Hence, from this statistical perspective, the adsorption capacity of the OFIC particles is primarily determined by the intrinsic properties of the material rather than by the specific lot. This result is particularly important considering that the sorbent used in this work is a waste biomass. As a result, the tested material exhibited robust reproducibility. A summary of the comparisons is provided in Table S7 of the Supplementary Materials.

3.5. Thermodynamic parameters of Pb^{2+} adsorption onto OFIC

The thermodynamic parameters ΔG^0, ΔH^0 and ΔS^0 of Pb^{2+} ions adsorption have been calculated by applying Gibbs and van't Hoff equations to the adsorption data recorded at pH = 5.0, without an ionic medium, at temperatures ranging from 284.15 to 318.15 K. In the chosen temperature range, the adsorption capacity of OFIC particles slightly decreases with the increasing of temperature, in agreement with Barka et al. [20]. An opposite trend was found for K_L values. The plot of ln K_L vs. −1/RT is reported in Figure S6 of Supplementary Materials, while the thermodynamic parameters values are collected in Table 6. The Pb^{2+} adsorption was a spontaneous process with $-\Delta G^0$ values in the range 25.7 – 30.1 kJ mol^{-1}. These values fall within the typical range (20–80 kJ mol^{-1}) of an ion-exchange based adsorption mechanism [75]. The adsorption process was endothermic, with a ΔH^0 value of 10.5 kJ mol^{-1}. ΔH^0 values lower than 40 kJ mol^{-1} are typical of a physical adsorption [54,76,77]. The positive entropy variation (ΔS^0 = 0.13 k J mol^{-1} K^{-1}) indicates an increasing degree of freedom of Pb^{2+} ions in solution and a dissociative mechanism of adsorption, probably due to the desolvation of lead ions, typical of physisorption [54,78]. The thermodynamic parameter values are in agreement with those found by Abrha et al. for the same adsorbent [45].

Table 6
Thermodynamic parameters ΔG^0, ΔH^0 and ΔS^0 for the Pb^{2+} adsorption onto OFIC from aqueous solution at pH = 5, in different ionic media, ionic strengths and temperatures.

T (K)	$-\Delta G^0$ [a]	ΔH^0 [a]	ΔS^0 [b]
284.15	25.7 ± 0.5	10.5 ± 0.7	0.13 ± 0.01
298.15	27.6 ± 0.5		
318.15	30.1 ± 0.5		

[a] kJ mol^{-1}
[b] kJ mol^{-1} K^{-1}

3.6. Comparison with literature data

The adsorption capacity and affinity of OFIC particles towards Pb^{2+} ions have been compared with those of several biomasses from literature [6,13,20–24,28,31]. The best-fit isotherm equation for the Pb^{2+} adsorption onto all the biomasses was the Langmuir model, whose parameter values are collected in Table S8 of the Supplementary Materials together with the relevant experimental conditions. In terms of maximum adsorption ability, the Diospyros kaki fallen leaves (DKFL) (q_m = 256 mg g^{-1} at pH = 5 and T = 303.15) [23] and the orange peel (OP) (q_m = 209.8 pH = 5 and T = 298.15 K) [21] have the highest q_m values, followed by six biomasses with q_m values in the range 110 – 150 mg g^{-1} [13,21,31], including OFIC particles (q_m = 113 mg g^{-1} at pH = 5 and T = 298.15 K) (see Fig. 10a). The q_m value of OFIC here reported is comparable to that obtained by Lavado-Meza et al. who used *Opuntia ficus indica* treated with NaOH 0.1 mol L^{-1} (q_m = 116.8 mg g^{-1} at pH = 4.5 and T = 293.15 K) [6]. For the same adsorbent, Abrha et al. found a q_m value of 62.89 mg g^{-1} at pH = 4 and T = 298.15 K. The lower q_m value is probably attributable to the different origins (Northern Ethiopia) and the use of the of larger OFIC particles up to 1.25 mm [45].

The choice of the best adsorbent material for the decontamination of polluted waters must be done by evaluating its adsorption capacity in the experimental conditions of the wastewater to be treated and, in particular, the pH, the ionic medium, the ionic strength, and the initial concentration (c_0) of the pollutant. In practice, waters polluted by toxic metal ions do not contain high concentrations of the metal [5] such as those usually reached in adsorption isotherm studies in which some authors use initial metal concentrations up to 1 g L^{-1} and in few cases higher [79]. For this reason, rather than relying on the q_m value, it is considered more useful to choose the most suitable adsorbent material on the basis of the q_e value corresponding to a c_0 value typical of polluted waters which usually does not exceed tens of mg L^{-1} (calculated using the values of the adsorption isotherm parameters). With this in mind, in Table S8 are also reported the adsorption abilities (q_e) of the biomasses for c_0 = 10 mg L^{-1}. At this Pb^{2+} concentration the best adsorbents are the Diospyros kaki fallen leaves DKFL (q_e = 9.9 mg g^{-1} at pH = 5 and T = 303.15 K) followed by OFIC with q_e = 9.71 mg g^{-1} at the same pH and at T = 298.15 K (see Fig. 10b). Also at this initial Pb^{2+} concentration the q_e value of OFIC is comparable with that obtained by Lavado-Meza et al. for the same adsorbent material treated with NaOH 0.1 mol L^{-1} (q_e = 9.74 mg g^{-1} at pH = 4.5 and T = 293.15 K) [6].

3.7. Breakthrough adsorption curves for the Pb^{2+} ions adsorption onto OFIC particles

Fixed-bed column experiments were carried out using Pb^{2+} aqueous solution at pH = 5.0, T = 298.15 K, without the addition of ionic medium, in $NaNO_3$ 0.1 mol L^{-1}, and in NaCl 0.1 and 0.5 mol L^{-1} (see Section 2.3 for experimental details). The collected data (c_t/c_0 vs t) were subjected to regression analysis by logistic (Eq. (12)), Gompertz (Eq. (13)) and Log-Gompertz (Eq. (14)) models. The results are shown in Fig. 11 and Figs. S5 – S7 of the Supplementary Materials together with the best fit curves of the three breakthrough models. The relevant fitting parameters are collected in Table S9 of Supplementary Materials together with the breakthrough times at c_t/c_0 = 0.5 ($BT_{0.5}$) calculated from best fit curve model. Moreover, other relevant design parameters

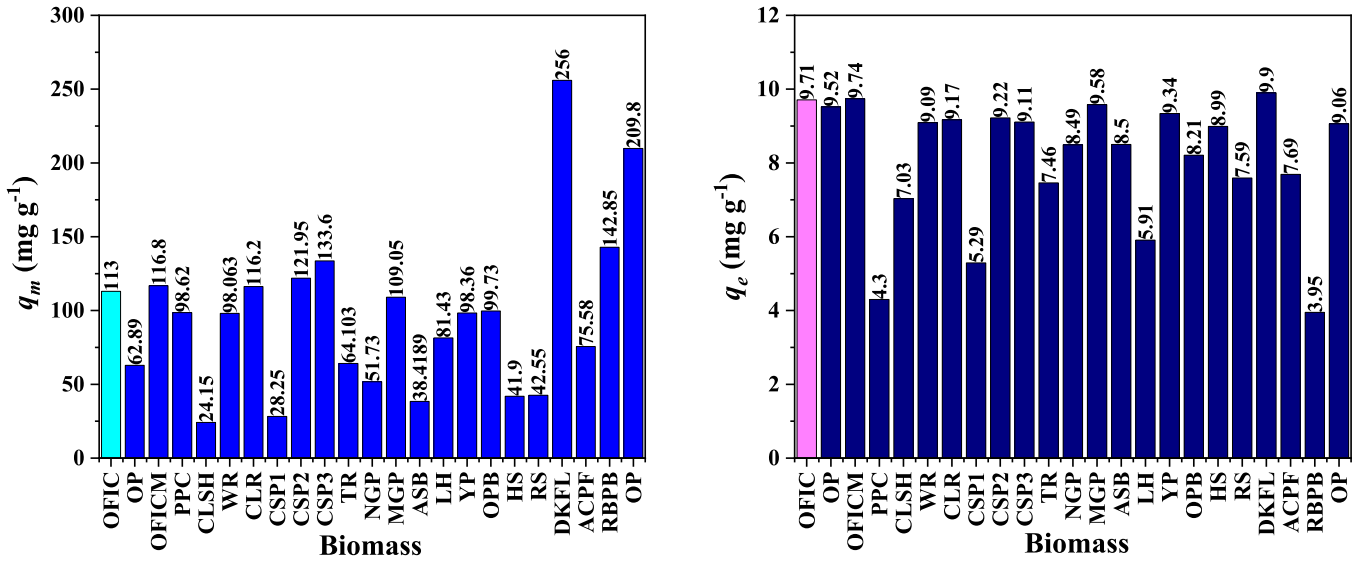

Fig. 10. Comparison of q_m and q_e (adsorption abilities of 1 g of the biomasses placed in 1 L of aqueous solution containing Pb^{2+} ions at concentration 10 mg L^{-1}) of literature biomasses.

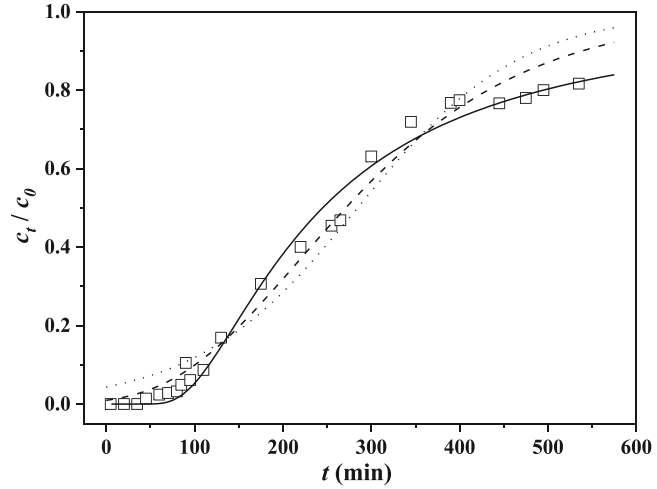

Fig. 11. Breakthrough curve of Pb^{2+} ions adsorption onto OFIC (90 mg) in aqueous solution at pH = 5.0, T = 298.15 K, c_0 = 5 mg L^{-1} and flow rate 3.25 mL min^{-1}. Experimental data were fitted to logistic (dot line), Gompertz (dashed line) and Log-Gompertz (continuous line) models.

for fixed-bed systems such as mass transfer zones (MTV), retardation factors (R), saturation points ($BT_{0.95}$), adsorption capacity under dynamic conditions (q_d), and adsorbent utilization (U%) [80–82] were calculated. The definition of these parameters is reported in the Supplementary Materials (Table S10) as well the obtained values (Table S11).

Irrespective of the experimental condition of Pb^{2+} solution, the metal ion is initially adsorbed by OFIC and, due to its progressive saturation, the breakthrough curve tends towards the unit value. The classic almost symmetric S-shaped breakthrough curve (Fig. 11) sometimes gives way to a strongly asymmetric S-shaped curve (Fig. S7) or to a monotonically increasing curve (Figs S8 – S9), approaching $c_t/c_0 = 1$, with a curvature depending on the experimental conditions.

The best breakthrough model, in terms of goodness of fit of experimental data, was the Log-Gompertz except for the breakthrough curve in $NaNO_3$ 0.1 mol L^{-1} for which the Gompertz model showed the highest adjusted R^2 value (see Table S9).

Although the empirical nature of these models does not allow to make considerations based on the values of their parameters, by choosing the best model for each data set, it is possible to calculate the parameter $BT_{0.5}$, i.e. the breakthrough time at which $c_t/c_0 = 0.5$ as well the other relevant design parameters for fixed-bed systems reported in Table S11. These parameters are useful both for a comparison between the various column experiments and for correlating the results of the column and batch adsorption experiments.

In particular, the $BT_{0.5}$ value is strongly influenced by the background salts, as well as their nature and concentration. The highest $BT_{0.5}$ value was obtained in the absence of an ionic medium. By adding an ionic medium at the same concentration (0.1 mol L^{-1}), NaCl reduces the $BT_{0.5}$ value to a greater extent than $NaNO_3$. When the NaCl concentration is increased to 0.5 mol L^{-1}, the $BT_{0.5}$ value is further reduced. The dependence of $BT_{0.5}$ and q_m on ionic strength and ionic medium is comparable (see Fig. 12), confirming that the adsorption behaviour of OFIC particles under equilibrium (batch experiments) and non-equilibrium (column) conditions is comparable.

The same considerations can be made by using, instead of $BT_{0.5}$, the retardation factor R, as R is defined by the ratio between the $BT_{0.5}$ and

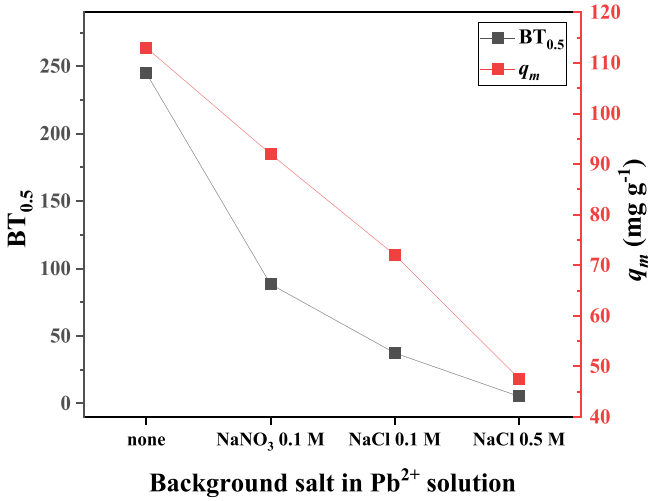

Fig. 12. Trend of the q_m and $BT_{0.5}$ parameters as a function of the ionic medium and ionic strength of the Pb^{2+} ions solutions in the batch and column experiments.

the constant quantity t_0 (i.e. the time of residence of non-retarded species). Looking at q_d and U% parameters, the sensitivity of these parameters to the background salt is more complex. In particular, q_d ranged from 64 mg g^{-1} in water to a value of approximately 20 mg g^{-1} in the presence of 0.1 mol L^{-1} of background salt, regardless of its nature, and was further reduced to 5.7 mg g^{-1} in 0.5 mol L^{-1} of NaCl.

3.8. Recycling and reuse of OFIC

The possibility of reusing the same adsorbent material multiple times proportionally reduces the costs of the decontamination process. For this reason, recycle and reuse experiments with OFIC particles have been carried out, performing four adsorption/desorption cycles (see Section 2.3 for experimental details). The adsorption and desorption q_e (mg g^{-1}) values found for the four cycles are depicted in the histogram of Fig. 13. The OFIC particles showed satisfactory reusability. In the first cycle, the q_e of adsorption and desorption reached the same values within the experimental uncertainties. In the three subsequent cycles, the adsorption ability of the adsorbent underwent a slight decrease, which did not exceed 15 % at the fourth cycle, and with complete desorption of the adsorbed toxic metal ion. The equilibrium adsorption capacity (q_e) values found in the four cycles, show that the regeneration efficiency slightly decreases from 89.3 % in the second cycle to 82.6 % in the fourth cycle. The complete desorption across the four adsorption /desorption cycles is a further experimental indication of the physisorption mechanism.

3.9. Adsorption mechanism of Pb^{2+} adsorption onto OFIC particles

Characterisation data, as well as adsorption results from batch and column experiments, outline a physical adsorption mechanism mainly based on electrostatic interactions of different strengths, and on ion exchange. In detail, SEM micrographs evidenced no significant changes on the surface of the material after Pb^{2+} adsorption. The toxic metal ion adsorption by OFIC was confirmed by semi quantitative analysis coming from EDX spectra that also showed a simultaneous release of Ca^{2+} ions. Considering the ATR-FTIR spectra, the new signals centered at 1569, 1288 and 772 cm^{-1} after Pb^{2+} adsorption unambiguous evidenced the interaction of the Pb^{2+} ions with the carboxylate groups and, to a lesser extent, with the hydroxyl groups of the biomass. The adsorption equilibrium was reached within 150/200 min with the kinetic well described

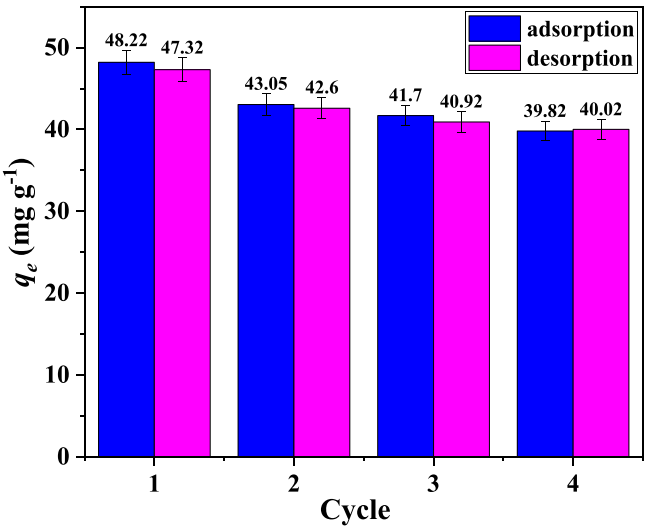

Fig. 13. q_e values of adsorption/desorption steps of Pb^{2+} ions onto OFIC particles. Experimental details: amount of OFIC ≈ 20 mg; Pb^{2+} ions solution: V = 15 mL, c_{Pb2+} = 65 mg L^{-1}, pH = 5.0 and T = 298.15 K; extractant solution: 15 mL of HCl 0.1 mol L^{-1}.

by the PSO model. The activation energy E_a = 24 kJ mol^{-1} is typical of physisorption. The Langmuir equation provided a better fitting of the adsorption isotherms ~~at~~ under every experimental condition. According to the isotherm model, the Pb^{2+} ions were mainly adsorbed by OFIC through equivalent sites, likely the carboxylic groups, that were saturated forming a monolayer on the surface of the adsorbent particles. The Ca^{2+} - Pb^{2+} ion exchange was confirmed by the gradual release of Ca^{2+} ions observed during two Pb^{2+}adsorption isotherm experiments (Fig. S5). The adsorption process was spontaneous ($25.7 \leq -\Delta G^0$ / kJ $mol^{-1} \leq 30.1$) and endothermic (ΔH^0 = 10.5 kJ mol^{-1}). The almost complete desorption of Pb^{2+} ions in the four cycles of recycling and reuse experiments confirms the weak Pb^{2+} - OFIC interactions typical of the physisorption-based mechanism.

3.10. Environmental impact and cost effectiveness of OFIC

Biosorption is widely acknowledged as a viable and eco-friendly approach for wastewater treatment. However, the scalability of the process depends not only on the adsorption performance of the adsorbent, but also on the economic feasibility, environmental impact, and the scalability of its production. Among these factors, the cost of the adsorbent is one of the key parameters, determining the overall sustainability of the process, as it is consistently highlighted in techno-economic assessments [83]. The possible production cost for 1 kg of OFIC, under laboratory conditions, can be roughly estimated at € 8.33 (see Table S12 of Supplementary Materials). Possible costs kept into account include the collection of agricultural waste (free of charge), 168 h of solar drying, a two-step washing process with tap water (~100 L) and deionized water (~20 L), respectively, 1.5 h of mechanical shaking, 48 h of oven drying at 333.15 K, and final grinding. The major cost contributors are oven drying (€ 6.48) and deionized water usage (€ 1.20), whereas the use of solar drying in the initial dehydration stage significantly reduces energy consumption and associated costs. Electricity costs were calculated based on the current average rate for non-domestic, low-voltage supply in Italy (€ 0.30 / kWh) [84]. When compared to more engineered materials, such as chemically modified adsorbents (e.g., biochar, acid/base-treated biomasses), which often exceed € 10–15/kg due to reagent costs, process complexity, and high energy demand, OFIC falls into a moderate-cost range. For instance, tangerine peel modified with sodium hydroxide has been reported to cost up to $ 18.51/kg, nearly three times higher than its unmodified counterpart ($ 5.26/kg) [85]. Similarly, adsorbents prepared from banana peel modified with surfactants have shown production costs of around $ 41/kg [86], both significantly higher than the market price of commercial activated carbon ($ 1.8–2.8/kg) [87]. The cost of OFIC is further justified by its favourable sustainability profile. No cultivation, harvesting, or chemical reagents are required, as *Opuntia ficus indica* cladodes are abundantly available as agricultural waste in Mediterranean area. Additionally, the production protocol avoids the use of hazardous substances, thereby reducing the environmental burden associated with treatment and disposal. Although the current estimated costs are based on the lab-scale production with no industrial-scale optimization, OFIC seems to be a promising adsorbent owing to its competitive cost and low environmental impact.

4. Conclusions

The *Opuntia ficus indica* particles have been successfully used as adsorbent material of Pb^{2+} ions. The adsorption equilibrium was reached within 150/200 min with a kinetic of adsorption well described by the PSO model. The activation energy value of 24 kJ mol^{-1} fell within the range typically associated with a physical adsorption mechanism based on ionic interactions of different strength and on ionic exchange with Ca^{2+} ions of the adsorbent. The adsorption capacity of OFIC was strictly dependent on the experimental conditions of the polluted water to be treated (ionic medium, ionic strength, pH,

temperature) and it was explained in terms of chemical speciation of Pb^{2+} ions, shielding effect and competition of the ions derived from background salts dissociation and protonation/deprotonation of binding sites of the adsorbent. ATR-FTIR spectra indicated a Pb^{2+} interaction with carboxylic and hydroxyl groups of OFIC. The adsorption isotherms were well described by Langmuir equation. The highest maximum adsorption capacity was found in solutions at pH = 5.0, $I \rightarrow 0$ mol L^{-1} and $T = 284.15$ K ($q_m = 121$ mg g^{-1}). The adsorption process was spontaneous, endothermic and characterised by a positive entropy change. Fixed-bed column experiments showed a comparable adsorption behaviour of OFIC particles under equilibrium and non-equilibrium conditions. The OFIC particles showed an excellent reuse capacity with a slightly decrease of the regeneration efficiency that was 82.6 % after four adsorption/desorption cycle. OFIC also has a competitive production cost (€ 8.33/kg) and a low environmental impact.

CRediT authorship contribution statement

Nicola Muratore: Writing – original draft, Investigation, Data curation. **Giulio Geraci:** Investigation. **Paolo Lo Meo:** Writing – review & editing, Writing – original draft, Supervision, Methodology, Investigation, Data curation. **Raccuia Salvatore:** Investigation, Data curation. **Rita Lo Brutto:** Investigation. **Marilena Tolazzi:** Investigation, Data curation. **Ettore Madonia:** Investigation. **Alberto Pettignano:** Writing – review & editing, Writing – original draft, Validation, Supervision, Investigation, Funding acquisition, Data curation, Conceptualization. **Davide Lascari:** Writing – original draft, Methodology, Investigation, Data curation, Conceptualization. **Andrea Melchior:** Investigation, Data curation. **Gabriele Lando:** Writing – review & editing, Writing – original draft, Methodology, Investigation, Data curation, Conceptualization. **Salvatore Cataldo:** Investigation, Data curation.

Declaration of Competing Interest

The authors declare that they have no known competing financial interests or personal relationships that could have appeared to influence the work reported in this paper.

Acknowledgments

The authors acknowledge the project supported by Next Generation EU, Missione 4, Componente 1, CUP: B53D23013740006—PRIN_2022HYH95P.

The authors also acknowledge the support of the National Recovery and Resilience Plan (NRRP), Mission 4 Component 2 Investment 1.4 - Call for tender No. 3138 of 16 December 2021, rectified by Decree n.3175 of 18 December 2021 of Italian Ministry of University and Research funded by the European Union –NextGeneration EU; Project code CN_00000033, Concession Decree No. 1034 of 17 June 2022 adopted by the Italian Ministry of University and Research, CUP B73C22000790001, Project title “National Biodiversity Future Center - NBFC”.

The authors thank the Professor Pellegrino Conte for his support in ATR-FTIR spectroscopy.

Appendix A. Supporting information

Supplementary data associated with this article can be found in the online version at doi:10.1016/j.jece.2025.118686.

Data availability

Data will be made available on request.

References

[1] T.R. Crompton, Toxicants in Aqueous Ecosystems: A Guide for the Analytical and Environmental Chemist, Springer Science & Business Media, 2006.
[2] S. Mnasri-Ghnimi, N. Frini-Srasra, Removal of heavy metals from aqueous solutions by adsorption using single and mixed pillared clays, Appl. Clay Sci. 179 (2019) 105151, https://doi.org/10.1016/j.clay.2019.105151.
[3] D.A. Gidlow, Lead toxicity, Occup. Med. 65 (2015) 348–356.
[4] K. Raj, A.P. Das, Lead pollution: impact on environment and human health and approach for a sustainable solution, Environ. Chem. Ecotoxicol. 5 (2023) 79–85, https://doi.org/10.1016/j.enceco.2023.02.001.
[5] V. Kumar, S.K. Dwivedi, S. Oh, A critical review on lead removal from industrial wastewater: recent advances and future outlook, J. Water Process Eng. 45 (2022) 102518, https://doi.org/10.1016/j.jwpe.2021.102518.
[6] C. Lavado-Meza, M.C. Fernandez-Pezua, F. Gamarra-Gómez, E. Sacari-Sacari, J. Angeles-Suazo, J.Z. Dávalos-Prado, Single and binary removals of Pb(II) and Cd (II) with chemically modified opuntia ficus indica cladodes, Molecules 28 (2023) 4451, https://doi.org/10.3390/molecules28114451.
[7] W. Liang, X. Wang, X. Zhang, L. Niu, J. Wang, X. Wang, X. Zhao, Water quality criteria and ecological risk assessment of lead (Pb) in China considering the total hardness of surface water: a national-scale study, Sci. Total Environ. 858 (2023) 159554, https://doi.org/10.1016/j.scitotenv.2022.159554.
[8] G.K. Kinuthia, V. Ngure, D. Beti, R. Lugalia, A. Wangila, L. Kamau, Levels of heavy metals in wastewater and soil samples from open drainage channels in Nairobi, Kenya: community health implication, Sci. Rep. 10 (2020) 8434, https://doi.org/10.1038/s41598-020-65359-5.
[9] Sustainable development goals, United Nations, Sustain. Dev. Goals (2025). ⟨https://sdgs.un.org/2030agenda⟩.
[10] W.S. Chai, J.Y. Cheun, P.S. Kumar, M. Mubashir, Z. Majeed, F. Banat, S.-H. Ho, P. L. Show, A review on conventional and novel materials towards heavy metal adsorption in wastewater treatment application, J. Clean. Prod. 296 (2021) 126589, https://doi.org/10.1016/j.jclepro.2021.126589.
[11] A. Ronda, M.A. Martín-Lara, E. Dionisio, G. Blázquez, M. Calero, Effect of lead in biosorption of copper by almond shell, J. Taiwan Inst. Chem. Eng. 44 (2013) 466–473.
[12] G. Crini, E. Lichtfouse, Advantages and disadvantages of techniques used for wastewater treatment, Environ. Chem. Lett. 17 (2019) 145–155, https://doi.org/10.1007/s10311-018-0785-9.
[13] I. Anastopoulos, I. Pashalidis, A. Hosseini-Bandegharaei, D.A. Giannakoudakis, A. Robalds, M. Usman, L.B. Escudero, Y. Zhou, J.C. Colmenares, A. Núñez-Delgado, É.C. Lima, Agricultural biomass/waste as adsorbents for toxic metal decontamination of aqueous solutions, J. Mol. Liq. 295 (2019) 111684, https://doi.org/10.1016/j.molliq.2019.111684.
[14] V.J. Landin-Sandoval, D.I. Mendoza-Castillo, A. Bonilla-Petriciolet, I.A. Aguayo-Villarreal, H.E. Reynel-Avila, H.A. Gonzalez-Ponce, Valorization of agri-food industry wastes to prepare adsorbents for heavy metal removal from water, J. Environ. Chem. Eng. 8 (2020) 104067, https://doi.org/10.1016/j.jece.2020.104067.
[15] L. Sánchez-Ponce, M. Díaz-de-Alba, M.J. Casanueva-Marenco, J. Gestoso-Rojas, M. Ortega-Iguña, M.D. Galindo-Riaño, M.D. Granado-Castro, Potential use of Low-Cost Agri-Food waste as biosorbents for the removal of Cd(II), Co(II), Ni(II) and Pb (II) from aqueous solutions, Separations 9 (2022) 309, https://doi.org/10.3390/separations9100309.
[16] N. El Messaoudi, Y. Miyah, Z.M. Şenol, Z. Ciğeroğlu, E.S. Kazan-Kaya, S. Gubernat, J. Georgin, D.S.P. Franco, Comprehensive analytical review of heavy metal removal efficiency using agricultural solid waste-based bionanocomposites, NanoStruct. NanoObjects 38 (2024) 101220, https://doi.org/10.1016/j.nanoso.2024.101220.
[17] S. Kainth, P. Sharma, O.P. Pandey, Green sorbents from agricultural wastes: a review of sustainable adsorption materials, Appl. Surf. Sci. Adv. 19 (2024) 100562, https://doi.org/10.1016/j.apsadv.2023.100562.
[18] Z. Phiri, N.T. Moja, T.T.I. Nkambule, L.-A. de Kock, Utilization of biochar for remediation of heavy metals in aqueous environments: a review and bibliometric analysis, Heliyon 10 (2024), https://doi.org/10.1016/j.heliyon.2024.e25785.
[19] P. Singh, U. Kumar, A. Dwivedi, P.K. Singh, I. Kumar, S. Mishra, A. Prajapati, S. Tiwari, R.K. Sharma, Green solutions for heavy metal remediation: unveiling the potential of agricultural waste through Techno-Economic analysis and life cycle assessment, in: Heavy Met. Contam. Environ, CRC Press, 2024.
[20] N. Barka, M. Abdennouri, M. El Makhfouk, S. Qourzal, Biosorption characteristics of cadmium and lead onto eco-friendly dried cactus (*Opuntia ficus indica*) cladodes, J. Environ. Chem. Eng. 1 (2013) 144–149, https://doi.org/10.1016/j.jece.2013.04.008.
[21] T.A.H. Nguyen, H.H. Ngo, W.S. Guo, J. Zhang, S. Liang, Q.Y. Yue, Q. Li, T. V. Nguyen, Applicability of agricultural waste and by-products for adsorptive removal of heavy metals from wastewater, Bioresour. Technol. 148 (2013) 574–585, https://doi.org/10.1016/j.biortech.2013.08.124.
[22] A. Şencan, M. Karaboyacı, M. Kılıç, Determination of lead(II) sorption capacity of hazelnut shell and activated carbon obtained from hazelnut shell activated with $ZnCl_2$, Environ. Sci. Pollut. Res. 22 (2015) 3238–3248, https://doi.org/10.1007/s11356-014-2974-9.
[23] R. Fan, Q. Yi, Y. Xie, F. Xie, Q. Zhang, Z. Luo, Enhanced adsorption and recovery of Pb(II) from aqueous solution by alkali-treated persimmon fallen leaves, J. Appl. Polym. Sci. 133 (2016), https://doi.org/10.1002/app.43656.
[24] H. Amer, A. El-Gendy, S. El-Haggar, Removal of lead (II) from aqueous solutions using rice straw, Water Sci. Technol. 76 (2017) 1011–1021, https://doi.org/10.2166/wst.2017.249.

[25] S. Cataldo, V. Chiodo, F. Crea, S. Maisano, D. Milea, A. Pettignano, Biochar from byproduct to high value added material – a new adsorbent for toxic metal ions removal from aqueous solutions, J. Mol. Liq. 271 (2018) 481–489.
[26] S. Cataldo, A. Gianguzza, D. Milea, N. Muratore, A. Pettignano, S. Sammartano, A critical approach to the toxic metal ion removal by hazelnut and almond shells, Environ. Sci. Pollut. Res. 25 (2018) 4238–4253, https://doi.org/10.1007/s11356-017-0779-3.
[27] Y. Dai, Q. Sun, W. Wang, L. Lu, M. Liu, J. Li, S. Yang, Y. Sun, K. Zhang, J. Xu, W. Zheng, Z. Hu, Y. Yang, Y. Gao, Y. Chen, X. Zhang, F. Gao, Y. Zhang, Utilizations of agricultural waste as adsorbent for the removal of contaminants: a review, Chemosphere 211 (2018) 235–253, https://doi.org/10.1016/j.chemosphere.2018.06.179.
[28] C. Tejada-Tovar, A.D. Gonzalez-Delgado, A. Villabona-Ortiz, Characterization of residual biomasses and its application for the removal of lead ions from aqueous solution, Appl. Sci. 9 (2019) 4486, https://doi.org/10.3390/app9214486.
[29] A.T. Hoang, S. Kumar, E. Lichtfouse, C.K. Cheng, R.S. Varma, N. Senthilkumar, P. Q. Phong Nguyen, X.P. Nguyen, Remediation of heavy metal polluted waters using activated carbon from lignocellulosic biomass: an update of recent trends, Chemosphere 302 (2022) 134825, https://doi.org/10.1016/j.chemosphere.2022.134825.
[30] A. Irto, S.G.M. Raccuia, G. Lando, C. De Stefano, K. Arena, T.M.G. Salerno, A. Pettignano, F. Cacciola, L. Mondello, P. Cardiano, Valorization of citrus waste for circular economy: a case study on bergamot pomace as sorbent for Cd^{2+}removal and source of added value compounds, Microchem. J. 193 (2023) 109183, https://doi.org/10.1016/j.microc.2023.109183.
[31] A. Alsulaili, K. Elsayed, A. Refaie, Utilization of agriculture waste materials as sustainable adsorbents for heavy metal removal: a comprehensive review, J. Eng. Res. 12 (2024) 691–703, https://doi.org/10.1016/j.jer.2023.09.018.
[32] Z. Hashmi, A.S. Jatoi, S. Nadeem, A. Anjum, S.M. Imam, H. Jangda, Comparative analysis of conventional to biomass-derived adsorbent for wastewater treatment: a review, Biomass. Convers. Biorefinery 14 (2024) 45–76, https://doi.org/10.1007/s13399-022-02443-y.
[33] N. Sheraz, A. Shah, A. Haleem, F.J. Iftikhar, Comprehensive assessment of carbon-, biomaterial- and inorganic-based adsorbents for the removal of the most hazardous heavy metal ions from wastewater, RSC Adv. 14 (2024) 11284–11310, https://doi.org/10.1039/D4RA00976B.
[34] R. Shoukat, M. Cappai, G. Pia, L. Pilia, An updated review: opuntia ficus indica (OFI) chemistry and its diverse applications, Appl. Sci. 13 (2023) 7724, https://doi.org/10.3390/app13137724.
[35] T. Nharingo, M. Moyo, Application of *opuntia ficus-indica* in bioremediation of wastewaters. A critical review, J. Environ. Manag. 166 (2016) 55–72, https://doi.org/10.1016/j.jenvman.2015.10.005.
[36] M. Barbera, S. Indelicato, D. Bongiorno, V. Censi, F. Saiano, D. Piazzese, Untreated opuntia ficus indica for the efficient adsorption of Ni(II), Pb(II), Cu(II) and Cd(II) ions from water, Molecules 28 (2023) 3953, https://doi.org/10.3390/molecules28093953.
[37] A. Attanzio, I. Restivo, M. Tutone, L. Tesoriere, M. Allegra, M.A. Livrea, Redox properties, bioactivity and health effects of indicaxanthin, a bioavailable phytochemical from opuntia ficus indica, L.: a critical review of accumulated evidence and perspectives, Antioxidants 11 (2022) 2364, https://doi.org/10.3390/antiox11122364.
[38] M. Aragona, E.R. Lauriano, S. Pergolizzi, C. Faggio, Opuntia ficus-indica (L.) miller as a source of bioactivity compounds for health and nutrition, Nat. Prod. Res. 32 (2018) 2037–2049, https://doi.org/10.1080/14786419.2017.1365073.
[39] M.F. Ramadan, T.E.M. Ayoub, S. Rohn (Eds.), Opuntia spp.: Chemistry, Bioactivity and Industrial Applications, Springer International Publishing, Cham, 2021, https://doi.org/10.1007/978-3-030-78444-7.
[40] J.M. Feugang, P. Konarski, D. Zou, F.C. Stintzing, C. Zou, Nutritional and medicinal use of cactus pear (Opuntia spp.) cladodes and fruits, Front. Biosci. J. Virtual Libr 11 (2006) 2574–2589, https://doi.org/10.2741/1992.
[41] G. Ginestra, M.L. Parker, R.N. Bennett, J. Robertson, G. Mandalari, A. Narbad, R. B. Lo Curto, G. Bisignano, C.B. Faulds, K.W. Waldron, Anatomical, chemical, and biochemical characterization of cladodes from prickly pear [Opuntia ficus-indica (L.) Mill.], J. Agric. Food Chem. 57 (2009) 10323–10330, https://doi.org/10.1021/jf9022096.
[42] H. Chahdoura, Z. Mzoughi, I. Ellouze, I. Generalić Mekinić, N. Čmiková, S. El Bok, H. Majdoub, A. Ben Hsouna, R. Ben Saad, W. Mnif, H. Mosbah, M. Ben M'hadheb, S. Garzoli, M. Kăcániová, *opuntia* species: a comprehensive review of chemical composition and bio-pharmacological potential with contemporary applications, South Afr. J. Bot. 174 (2024) 645–677, https://doi.org/10.1016/j.sajb.2024.09.038.
[43] A. Maceda, M. Soto-Hernández, C.B. Peña-Valdivia, C. Trejo, T. Terrazas, Characterization of lignocellulose of opuntia (Cactaceae) species using FTIR spectroscopy: possible candidates for renewable raw material, Biomass. Convers. Biorefinery 12 (2022) 5165–5174, https://doi.org/10.1007/s13399-020-00948-y.
[44] A. Bernardino-Nicanor, J.L. Montañez-Soto, E. Conde-Barajas, M. de la, L. X. Negrete-Rodríguez, G. Teniente-Martínez, E.A. Vargas-León, J.M.S. Juárez-Goiz, G. Acosta-García, L. González-Cruz, Spectroscopic and structural analyses of opuntia robusta mucilage and its potential as an edible coating, Coatings 8 (2018) 466, https://doi.org/10.3390/coatings8120466.
[45] Y.W. Abrha, Y. Ahn, H. Kye, Y. Jung, Y. Yoon, T.-M. Hwang, J.-W. Kang, Adsorption of Pb2+ and Zn2+from aqueous solutions using dried powder of cactus opuntia: characterization, adsorption capacity and kinetics, Desalin. Water Treat. 135 (2018) 330–340, https://doi.org/10.5004/dwt.2018.22309.
[46] D. Kumar, L.K. Pandey, J.P. Gaur, Metal sorption by algal biomass: from batch to continuous system, Algal Res 18 (2016) 95–109, https://doi.org/10.1016/j.algal.2016.05.026.
[47] S. Lagergren, About the theory of so called adsorption of soluble substances, K. Sven. Vetensk. Handl. 24 (1898) 1–39.
[48] U. Wingenfelder, C. Hansen, G. Furrer, R. Schulin, Removal of heavy metals from mine waters by natural zeolites, Environ. Sci. Technol. 39 (2005) 4606–4613, https://doi.org/10.1021/es048482s.
[49] K.L. Tan, B.H. Hameed, Insight into the adsorption kinetics models for the removal of contaminants from aqueous solutions, J. Taiwan Inst. Chem. Eng. 74 (2017) 25–48, https://doi.org/10.1016/j.jtice.2017.01.024.
[50] H.M.F. Freundlich, Uber die adsorption in losungen, Z. Phys. Chem. Leipz. 57 (1906) 385–470.
[51] I. Langmuir, The adsorption of gases on plane surfaces of glass, mica and platinum, J. Am. Chem. Soc. 40 (1918) 1361–1403, https://doi.org/10.1021/ja02242a004.
[52] Y. Liu, Is the free energy change of adsorption correctly calculated? J. Chem. Eng. Data 54 (2009) 1981–1985, https://doi.org/10.1021/je800661q.
[53] G. Crini, P.-M. Badot, Application of chitosan, a natural aminopolysaccharide, for dye removal from aqueous solutions by adsorption processes using batch studies: a review of recent literature, Prog. Polym. Sci. 33 (2008) 399–447, https://doi.org/10.1016/j.progpolymsci.2007.11.001.
[54] H.N. Tran, S.-J. You, H.-P. Chao, Thermodynamic parameters of cadmium adsorption onto Orange peel calculated from various methods: a comparison study, J. Environ. Chem. Eng. 4 (2016) 2671–2682, https://doi.org/10.1016/j.jece.2016.05.009.
[55] D. Juela, M. Vera, C. Cruzat, X. Alvarez, E. Vanegas, Mathematical modeling and numerical simulation of sulfamethoxazole adsorption onto sugarcane bagasse in a fixed-bed column, Chemosphere 280 (2021) 130687, https://doi.org/10.1016/j.chemosphere.2021.130687.
[56] Q. Hu, Z. Zhang, Comment on ″Exponential and logistic functions: the two faces of the Bohart–Adams model″, J. Hazard. Mater. 394 (2020) 122508 https://doi.org/10.1016/j.jhazmat.2020.122508.
[57] Q. Hu, X. Yang, L. Huang, Y. Li, L. Hao, Q. Pei, X. Pei, A critical review of breakthrough models with analytical solutions in a fixed-bed column, J. Water Process Eng. 59 (2024) 105065, https://doi.org/10.1016/j.jwpe.2024.105065.
[58] F. Crea, C. De Stefano, A. Gianguzza, A. Pettignano, D. Piazzese, S. Sammartano, Acid−Base properties of synthetic and natural polyelectrolytes: experimental results and models for the dependence on different aqueous Media†, J. Chem. Eng. Data 54 (2009) 589–605, https://doi.org/10.1021/je800518j.
[59] C.De Stefano, C. Mineo, C. Rigano, S. Sammartano, Ionic strength dependence of formation constants. Xvii. the calculation of equilibrium concentrations and formation constants, Ann. Chim. Rome 83 (1993) 243–277.
[60] S.G.M. Raccuia, E. Zanda, C. Bretti, M. Formica, E. Macedi, A. Melchior, M. Tolazzi, M. Sanadar, D. Lascari, G. De Luca, A. Irto, C. De Stefano, P. Cardiano, G. Lando, Multi-Analytical approach for the Acid-Base, thermal and surface properties assessment of waste biomasses, Molecules 29 (2024) 5735, https://doi.org/10.3390/molecules29235735.
[61] Y. Horikawa, S. Hirano, A. Mihashi, Y. Kobayashi, S. Zhai, J. Sugiyama, Prediction of lignin contents from infrared spectroscopy: chemical digestion and Lignin/Biomass ratios of cryptomeria japonica, Appl. Biochem. Biotechnol. 188 (2019) 1066–1076, https://doi.org/10.1007/s12010-019-02965-8.
[62] www.chemicalbook.com, Lead acetate trihydrate(6080-56-4) IR Spectrum, (2025). https://www.chemicalbook.com/SpectrumEN_6080-56-4_IR1.htm.
[63] S. Cazalbou, G. Bertrand, C. Drouet, Tetracycline-Loaded biomimetic apatite: an adsorption study, J. Phys. Chem. B 119 (2015) 3014–3024, https://doi.org/10.1021/jp5116756.
[64] L. Largitte, R. Pasquier, A review of the kinetics adsorption models and their application to the adsorption of lead by an activated carbon, Chem. Eng. Res. Des. 109 (2016) 495–504, https://doi.org/10.1016/j.cherd.2016.02.006.
[65] M. Al-Ghouti, M.A.M. Khraisheh, M.N.M. Ahmad, S. Allen, Thermodynamic behaviour and the effect of temperature on the removal of dyes from aqueous solution using modified diatomite: a kinetic study, J. Colloid Interface Sci. 287 (2005) 6–13, https://doi.org/10.1016/j.jcis.2005.02.002.
[66] T.S. Anirudhan, P.G. Radhakrishnan, Thermodynamics and kinetics of adsorption of Cu(II) from aqueous solutions onto a new cation exchanger derived from tamarind fruit shell, J. Chem. Thermodyn. 40 (2008) 702–709, https://doi.org/10.1016/j.jct.2007.10.005.
[67] V.J. Inglezakis, A.A. Zorpas, Heat of adsorption, adsorption energy and activation energy in adsorption and ion exchange systems, Desalin. Water Treat. 39 (2012) 149–157, https://doi.org/10.5004/dwt.2012.3000.
[68] H. Nollet, M. Roels, P. Lutgen, P. Van der Meeren, W. Verstraete, Removal of PCBs from wastewater using Fly ash, Chemosphere 53 (2003) 655–665, https://doi.org/10.1016/S0045-6535(03)00517-4.
[69] M.E. Argun, Use of clinoptilolite for the removal of nickel ions from water: kinetics and thermodynamics, J. Hazard. Mater. 150 (2008) 587–595, https://doi.org/10.1016/j.jhazmat.2007.05.008.
[70] M. Doğan, H. Abak, M. Alkan, Adsorption of methylene blue onto hazelnut shell: kinetics, mechanism and activation parameters, J. Hazard. Mater. 164 (2009) 172–181, https://doi.org/10.1016/j.jhazmat.2008.07.155.
[71] S. Chakravarty, A. Mohanty, T.N. Sudha, A.K. Upadhyay, J. Konar, J.K. Sircar, A. Madhukar, K.K. Gupta, Removal of Pb(II) ions from aqueous solution by adsorption using bael leaves (*Aegle marmelos*), J. Hazard. Mater. 173 (2010) 502–509, https://doi.org/10.1016/j.jhazmat.2009.08.113.
[72] C. Wang, G. Lin, J. Zhao, S. Wang, L. Zhang, Enhancing Au(III) adsorption capacity and selectivity via engineering MOF with mercapto-1,3,4-thiadiazole, Chem. Eng. J. 388 (2020) 124221, https://doi.org/10.1016/j.cej.2020.124221.

[73] B. Volesky, Sorption and Biosorption, BV Sorbex, Inc., Montréal, St. Lambert, Québec, Canada, 2003.
[74] Y. Luo, F.J. Millero, Stability constants for the formation of lead chloride complexes as a function of temperature and ionic strength, Geochim. Cosmochim. Acta 71 (2007) 326–334.
[75] G. Gereli, Y. Seki, İ. Murat Kuşoğlu, K. Yurdakoç, Equilibrium and kinetics for the sorption of promethazine hydrochloride onto K10 montmorillonite, J. Colloid Interface Sci. 299 (2006) 155–162, https://doi.org/10.1016/j.jcis.2006.02.012.
[76] G. Gereli, Y. Seki, İ. Murat Kuşoğlu, K. Yurdakoç, Equilibrium and kinetics for the sorption of promethazine hydrochloride onto K10 montmorillonite, J. Colloid Interface Sci. 299 (2006) 155–162, https://doi.org/10.1016/j.jcis.2006.02.012.
[77] Y. Liu, Y.-J. Liu, Biosorption isotherms, kinetics and thermodynamics, Sep. Purif. Technol. 61 (2008) 229–242, https://doi.org/10.1016/j.seppur.2007.10.002.
[78] F. Ramezani, H. Rafii-Tabar, An in-depth view of human serum albumin corona on gold nanoparticles, Mol. Biosyst. 11 (2015) 454–462, https://doi.org/10.1039/c4mb00591k.
[79] S. Yadav, A. Yadav, N. Bagotia, A.K. Sharma, S. Kumar, Adsorptive potential of modified plant-based adsorbents for sequestration of dyes and heavy metals from wastewater - a review, J. Water Process Eng. 42 (2021) 102148, https://doi.org/10.1016/j.jwpe.2021.102148.
[80] D.C. Bouchard, A.L. Wood, M.L. Campbell, P. Nkedi-Kizza, P.S.C. Rao, Sorption nonequilibrium during solute transport, J. Contam. Hydrol. 2 (1988) 209–223, https://doi.org/10.1016/0169-7722(88)90022-8.
[81] X. Zhang, Y. Liang, T. You, L. Tian, G. Xu, C. Yang, J. Xiao, M. Tang, The influence of activated carbon fiber paper structure on adsorption performance of cyclohexane, Sep. Purif. Technol. 348 (2024) 127740, https://doi.org/10.1016/j.seppur.2024.127740.
[82] H. Matharage, M. Jayaweera, N. Bandara, J. Manatunge, D. Jayawardana, J. Dissanayake, Fixed-bed column studies on the adsorption of bisphenol a from aqueous solutions using chemically activated king coconut biochar, Discov. Chem. Eng. 5 (2025) 9, https://doi.org/10.1007/s43938-025-00082-z.
[83] N. Karić, A.S. Maia, A. Teodorović, N. Atanasova, G. Langergraber, G. Crini, A.R. L. Ribeiro, M. Đolić, Bio-waste valorisation: agricultural wastes as biosorbents for removal of (in)organic pollutants in wastewater treatment, Chem. Eng. J. Adv. 9 (2022) 100239, https://doi.org/10.1016/j.ceja.2021.100239.
[84] ARERA, Relazione annuale 2023–2024. Prezzo medio energia elettrica per usi non domestici, bassa tensione, (2024). ⟨https://www.arera.it/fileadmin/allegati/relaz_ann/25/Sintesi_Relazione_Annuale_2025_16giu.pdf⟩.
[85] L.M.S. Batista, J.A.T. Barboza, T.F. Souza, A.B. Mageste, I.A. Marques, L.L.B. S. Nascimento, L.H.M. da Silva, G.M.D. Ferreira, Tangerine peel modified with sodium hydroxide for the removal of methylene blue: a calorimetric approach, Colloids Surf. Physicochem. Eng. Asp. 704 (2025) 135423, https://doi.org/10.1016/j.colsurfa.2024.135423.
[86] J.A.T. Barboza, E.S. Penido, G.M.D. Ferreira, Production of surfactant-modified banana peel biosorbents applied to treatment and decolorization of effluents, Colloids Surf. Physicochem. Eng. Asp. 680 (2024) 132650, https://doi.org/10.1016/j.colsurfa.2023.132650.
[87] Z. Mahdi, A. El Hanandeh, Q.J. Yu, Preparation, characterization and application of surface modified biochar from date seed for improved lead, copper, and nickel removal from aqueous solutions, J. Environ. Chem. Eng. 7 (2019) 103379, https://doi.org/10.1016/j.jece.2019.103379.